Fold-and-thrust belt deformation of the Hongliuhe Group: a Permian tectonic closure record of the Central Asian Orogenic Belt, NW China

by
Nathan Cleven

A thesis

presented to the University of Waterloo

in fulfilment of the

thesis requirement for the degree of

Master of Science

in

Earth Sciences

Waterloo, Ontario, Canada, 2011

I hereby declare that I am the sole author of this thesis. This is a true copy of the thesis, including any required final revisions, as accepted by my examiners.

I understand that my thesis may be made electronically available to the public.

Abstract

The Early Permian strata of the Hongliuhe Group, NW China, experienced a thin-skinned fold-and-thrust belt style of deformation that recorded the final stages of amalgamation of the Beishan orogenic collage, a part of the Central Asian Orogenic Belt. The Hongliuhe Group was syn-orogenically deposited on an undetermined foreland, with the Mazongshan arc terrane acting as the hinterland. In this study results from detailed mapping combined with a regional analysis elucidate involvement of a northward-dipping subduction system with the collision.

Well-preserved fold-and-thrust belt style deformation mapped in the upper stratigraphy of the Hongliuhe Group exhibits dominantly south-southeast verging structure, including shear folding, low-angle thrust ramping, imbrication and duplexing. Restoration of a portion of a mapped outcrop-scale cross-section estimates the accommodation of a minimum of 24% shortening. Lower stratigraphy shows discrete, steeper, north-over-south dip-slip ductile shear zones that bound packages of less deformed Hongliuhe Group strata. Fault displacement is considered to have been prolonged enough to juxtapose basal formations in northerly hangingwalls against upper formations in southerly footwalls. Faulting is closely associated with the creation of large-scale brittle-ductile eye-fold structures that are postulated to be sheath folds. The most examined and mapped structure, 16km wide, is a synclinal structure with axes plunging steeply towards its center. The ellipticity of the exposed bedding traces increases towards the center of the eye-fold, implying a structural relationship with metamorphic shear zones. Except for large-scale folding, the bulk of its strata remain relatively undeformed and have preserved primary soft-sediment deformation structures indicating younging towards the center on both limbs of the synclinal structure.

Stratigraphic reconstruction of the Hongliuhe Group that considers the significant faulting shows that the Group's basal conglomerates unconformably overlie a Late-Carboniferous volcanic assemblage. The clast lithotypes of the conglomeratic successions change from polymictic metamorphic rocks at the base to monomictic granitoid clasts mid-section, showing the gradual unroofing sequence of the provenance. The stratigraphic reconstruction shows a general fining upward sequence, transitioning from terrestrial to nearshore marine depositional environments that, and in conjunction with the conglomeratic successions, suggests that the tectonic setting for deposition of the Hongliuhe Group is a foreland basin. Considering the deformation styles reported in this study, the Hongliuhe Group is interpreted to be a foreland fold-and-thrust belt.

Acknowledgements

I would like to thank my friends, family and colleagues that have provided me with incredible inspiration over the years. It is important to me to acknowledge the help and support of the Chinese students and professors that have assisted me in my field work, especially Ao Songjian, Tian Zhonghua and Ma Chong for their invaluable help in the field, and Professor Xiao Wenjiao for his generous support of my work. Thank you Joanna Hamlyn for being my field assistant in the summer of 2009 and sticking through it. The help from Professor Jin Jisuo from University of Western Ontario with Chinese translations was especially helpful and much appreciated. Many thanks to my committee, Bob Linnen and Mario Coniglio, and to Shoufa Lin, my advisor.

Table of Contents

List of Figures

1 Introduction

1.1 Introduction

Foreland fold-and-thrust belts are important structural features that mark the external limits of deformation processes in collisional orogenies. They provide important information and evidence of subduction processes and effects on lithologies, as well as the timing of tectonic collision. The presence of concurrently developed folding and thrusting in sedimentary rocks shed from a building and uplifting arc yields clues to rates of orogenic uplift and the horizontal motion of colliding continents. Vergence of the collision-induced structures in the forearc mimics that of the down-going slab and provides framework for the interpretation of the cryptic structural associations encountered in a suture zone (Windley et al., 2007). Fold-and-thrust belts have provided a fundamental basis for our understanding of the morphology of an exhumed tectonic collision zone and its associated subduction system.

The foreland basin deposits that host the fold-and-thrust belts are the last expression of a collisional orogenic system and provide constraints on the timing of tectonic collision. Final bouts of uplift from collision provides a source and the gravitic transport mechanism for high erosion and sedimentation rates into the early, shallow foreland basin. With time, and contraction of the basin, the combined effects of sediment accumulation and thrust-stacking of the supracrustal rocks induces downward lithospheric flexure (Covey, 1986; DeCelles and Giles, 1996). Also theorized to contribute to subsidence are the mountain load from collision and the pull of the dense subducted slab still attached to the overridden plate (DeCelles and Giles, 1996). All of these subsidence forces cause a progressively deepening depositional environment, from terrestrial to oceanic, giving a transition that is unique to the foreland area of a tectonic collision (Cross, 1986). The sedimentary successions produced provide a history of the unroofing of the orogeny. This synchronous contraction and thickening through thrust faulting creates a dynamic interplay with subsidence that allow geologists to interpret the ages of tectonism, depositional setting and provenances.

1.1.1 Location and Accessibility

This study of a foreland fold-and-thrust belt was conducted in the Beishan region, located in Northwest China. The Beishan region straddles the border between the Xinjiang Autonomous Region and Gansu Province. While its name translates to *Northern Mountains* the topographic relief in the Beishan region is minimal, in the low scale of hundreds of meters. The area contains small, disparate mountain chains of a multitude of geologic origins. The climate is arid desert,

and vegetation is minimal to non-existent, which allows excellent exposure and accessibility of outcrop. Desert regolith and unconsolidated lacustrine deposits cover areas between outcrop exposures. In summer months there are almost no standing bodies of water, and river beds are typically dry. The nearest regional airport is in the city of Dunhuang, a tourist frequented city, an hour's drive south of the Beishan. The small mining town of Liuyuan has a rail station that provides rail service northwest to the major cities in Xinjiang, and southeast to Beijing and the rest of China.

1.1.2 Previous Work

Early work in the Beishan has mainly been from large-scale tectonics projects in the Central Asian Orogenic Belt. The location is between the Tarim block and the North China craton. Studies of the tectonic history of those terranes has been conducted extensively over the previous two decades, and many of the studies interpreted the Beishan as a promontory of the Tarim or as extensions of the Mongolian or Tianshan orogenies (Charvet et al., 2007; Xiao et al., 2009b). The work of Xiao et al. (2011) is the first to provide a comprehensive tectonostratigraphic framework of the Beishan.

The Hongliuhe Group, which contains the fold-and-thrust belt examined in this study, has rarely, if at all, been included in the large-scale works mentioned above. However, it has been studied stratigraphically many times since 1958, and most recently in 2006 (Li et al., 2006 and references therein) whereby it was elevated to 'Group' status from its previous status as a 'Formation'. This report will draw upon the stratigraphic classification of Li et al. (2006) for the Hongliuhe Group.

1.1.3 Geologic Mapping in the Hongliuhe Area

Field work was carried out over two seasons and consisted of foot and vehicle traverses along and off rural roads in the area. The rail town of Liuyuan was used as a staging ground for multi-day expeditions to the Hongliuhe area. Though a small town exists within the map area, named Hongliuhe, at the time of the field work it was without sources of electricity or water making it unsuitable for lodging or resupplying.

During mapping efforts lithologies were noted, mapped, photographed and sampled. Samples were taken for discrimination of cryptic lithologies and for structural purposes, namely the kinematics of fault zones. Thin sections were cut and petrographic techniques were used to establish lithologies, metamorphism, alteration, and the effects and mechanisms of defor-

mation. Map production included a 1:50 000 scale geologic map covering an area 60x35 km, and a 136.5 m long 1:50 scale structural cross-sectional map of a road-cut outside the 1:50 000 mapped area, in the Hongliuhe Group, near the town of Xingxingxia.

1.2 Purpose of Study

This study is a structural analysis of a portion of a tectonic accretionary zone, of fold-and-thrust belt style deformation in the foreland basin of a Late Paleozoic arc-arc collision in northwest China. The importance of this foreland deposit, part of the Hongliuhe Group (Hongliuhe translates as *'Red Willow River'*, a river than runs through the area in modern times), is that its creation and fold-and-thrust belt deformation marks and constrains one of the youngest episodes of tectonic closure in the Beishan orogenic collage, which itself is one of the final episodes of accretion within the Central Asian Orogenic Belt.

1.3 Geologic Setting: The Central Asian Orogenic Belt

The Beishan orogenic collage is part of a larger scale accretionary orogenic belt termed the Central Asian Orogenic Belt (CAOB) (Fig. 1). This name is relatively new, with respect to its

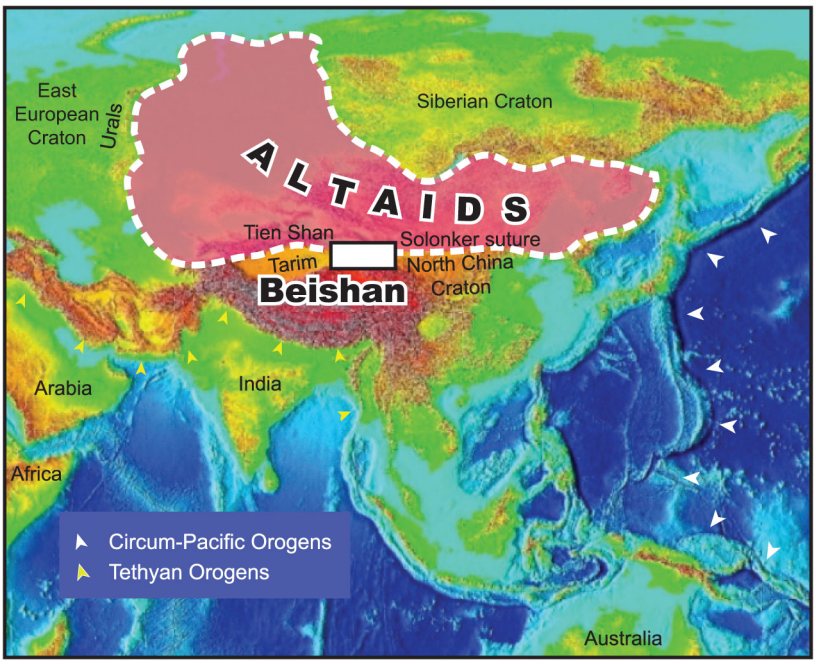

Figure 1: The Central Asian Orogenic Belt, also known as the Altaids, spans Russia, Kazakhstan, China and Mongolia. The area of this study is in the southern portion of the orogenic belt, within the inset box. The inset box is the location of Figure 2. (From Xiao et al., 2011)

history of study, and was proposed to reflect the larger portion of Asia that modern systems of research have established are related to its tectonic history. It has historically been referred to as the Altaids, a term coined by Eduard Suess in 1901 (Şengör and Natal'in, 2007) to define the related orogenies between the Siberia and Baltica cratons. Since the introduction of modern plate tectonics in the 1950's and 1960's, and tectonostratigraphic terrane analysis in the 1980's and 1990's, workers have shown that orogenic events spanning Kazakhstan in the West, Mongolia in the East, Siberia in the North, and Northern China in the south are all related to one long-lived orogenic system derived from subduction of the Paleo-Asian ocean. The CAOB is an east-west trending, southward younging orogenic collage that is geographically constrained by the Siberia and Baltica (East European) cratons in the North and the Tarim and North China cratons in the South (Xiao et al., 2003) (Fig. 1). Orogenic development began c. 1.0 Ga and continued to its termination in the Permian in the west (Windley et al., 2007) and Early Jurassic in the East (Xiao et al., 2003). Estimates state that subduction systems in the CAOB account for approximately 48% of the Earth's total of new continental crust generated in the Paleozoic. (Şengör et al., 1993)

Previous to the opening of China to western researchers in the 1980's, world plate tectonic maps divided northwest China into the Eurasian plate or the North China plate, with little regard for actual tectonic boundaries (Coleman, 1989). Early work in the late 1980's and 1990's to bring tectonic models for the CAOB into modern terms hinged on identifying terranes of the orogenic system and establishing their boundaries (Coleman, 1989; Windley et al., 1990; Allen et al., 1992; Şengör et al., 1993). The work of Coleman (1989) laid the groundwork for identification of terrane domains of oceanic crust, continental crust, island arc crust, and composite crust, with the major bounding faults, through synthesis of Chinese maps and literature with modern tectonic theory. A key finding that established a loose framework for interpretation of the orogenic belt was the wide geographical distribution of Late Paleozoic A-type granites, showing the general timing of final amalgamation. These Carboniferous and Permian post-collisional granites are distributed along all major orogenies and suture zones in the CAOB.

It was from this basis two distinct models of tectonic amalgamation developed and have been debated since: the single arc model and the island archipelago model.

The 'Kipchak arc' model proposes that the development of all individual orogens of the CAOB were the result of one to three oceanward-migrating arcs (Şengör et al., 1993; Yakubchuk, 2004; Wang et al., 2003). The main arc, the 'Kipchak arc', was proposed to have initiated west-dipping subduction off of a conjoined front of the Siberia and Baltica cratons in the Vendian

to Cambrian periods. Oceanward migration of the magmatic front throughout the Paleozoic was provided as an explanation for the (present day) southward-younging of the orogenic belt. Convergence between the two cratons, constant westward-subduction under the east side of the landmasses, and some strike-slip shuffling allowed for their reconstruction to resemble the morphology of the CAOB by Late Permian time. The island archipelago model developed from detailed work by Chinese and western European workers that showed that there must have been multiple independent subduction events of different polarities (Coleman, 1989; Windley et al., 1990; Gao et al., 1998; Laurent-Charvet et al., 2003). Modern paleomagnetic data has allowed for reinterpretation of the positions of Baltica and Siberia in the Early Cambrian – on different sides of the equator, separated by at least 1000 km – disallowing the close proximity required for the single arc model (Windley et al., 2007). Research into the main orogens in the CAOB has shown there to be three independent larger scale mountain belts: the Altay mountains (Zhang et al., 1993; Laurent-Charvet et al., 2002, 2003; Windley et al., 2002; Xiao et al., 2004a; Wang et al., 2003, 2006; Xiao et al., 2008; Briggs et al., 2009), the Tianshan (Coleman, 1989; Windley et al., 1990; Gao et al., 1998; Chen et al., 1999; Laurent-Charvet et al., 2002; Xiao et al., 2004b, 2009b), and the Mongol-Okhotsk (Li et al., 2002; Xiao et al., 2003; Windley et al., 2007; Xiao et al., 2009a).

Many of the arcs associated with these orogenies did not accrete directly against the Siberian margin as they were buffered by a series of terranes between them. These terranes, such as the island arcs of the Junggar and the Beishan, are the main evidence for the island archipelago model. The origins of the island arc terranes vary to a large degree, as separated forearcs of the Tianshan and Altay, as intra-oceanic island arcs and as accretionary complexes through which arc magmatism has migrated (Zhang et al., 1993; Allen et al., 1995; Buckman and Aitchison, 2004; Xiao et al., 2004b; Charvet et al., 2007; Xiao et al., 2009a,b).

The timing of the final amalgamation event of the North China craton to the terranes to its north has been constrained to the Middle Permian in the west (Windley et al., 1990; Gao et al., 1998; Chen et al., 1999; Laurent-Charvet et al., 2002; Xiao et al., 2004b, 2009b), and Late Permian to Lower Jurassic (Li et al., 2002; Xiao et al., 2003; Windley et al., 2007; Xiao et al., 2009a) in the east. The suture zone that records this is the Solonker suture (Xiao et al., 2003, 2009a), which when traced westward, connects with the South Tianshan suture, the suture that records the final closing between the Tarim/Tianshan and the active margin of the Siberian craton. This connection along the Solonker–South Tianshan sutures implies that, even though the North China craton docked later than the Tarim, the mechanisms of their final accretion have a direct relationship. The Beishan lies directly between these two

cratons, and its complicated tectonic history has been glossed over by most studies to date yet promises to provide many details about the final closure of the Central Asian Orogenic Belt.

1.4 Tectonic Setting: The Beishan Orogenic Collage

The Beishan Orogenic Collage is a group of arc terranes caught in a complicated zone between two major cratons accreting to the Central Asian Orogenic Belt. Most research to date has associated the terranes of the Beishan with the Eastern Tianshan and used explanations such as the Beishan being a promontory of the Tarim craton to provide a cratonic backing for final accretion. The recent work of Xiao et al. (2011) provides a framework for tectonic classification of the terranes in the Beishan (Fig. 2). The terranes of the Beishan can be traced west to where they share boundaries with terranes of the Tianshan. Similarly they can be traced east to their shared border with terranes associated with the Mongolian accretionary complexes, though they have independent tectonic histories from either. The Dunhuang block, a poorly understood assumed Precambrian cratonic block, accreted northwards onto the Siberian active margin in the Permian; both margins were active, with subduction facing south under the Dunhuang block, and north under the Siberian active margin. The continental arc produced in the Dunhuang block is called the Shibanshan arc (southernmost arc in Fig. 2, labelled '9') and in the north the Queershan arc was built in the Siberian active margin (northernmost arc in Fig. 2, labelled '1') (Xiao et al., 2011).

During the Late Carboniferous and Early Permian the terranes between these two continental margins were an already developed arc accretionary complex, termed the Gongpoquan accretionary complex by Xiao et al. (2011). The Hongliuhe Group lies within this accretionary complex, more specifically within the Mazongshan arc terrane boundaries (Fig. 2, unit labelled '5'). The Mazongshan arc is an Early to Middle Paleozoic volcanic arc and is separated from the Hanshan arc to its north by the Xingxingxia and Shibanjing ophiolitic mélanges. It is separated from the Shuangyingshan-Huaniushan arc (a late Proterozoic arc intruded by late Paleozoic plutons) to its south by the Hongliuhe and Xichangjing ophiolitic mélanges (Fig. 2). These arcs were assembled into the middle stage of the Gongpoquan arc-accretionary system by the Devonian to Early Carboniferous according to the tectonic model proposed by Xiao et al. (2011) ('Phase II' in Fig. 3). The model continues to show the next stage, 'Phase III', whereby all of the arcs between the two cratons joined to form the 'mature' Gongpoquan arc-accretionary system in the Late Carboniferous to Early Permian. This point in the development of the Beishan is the most relevant to this study. There is a note under 'Phase III' in Figure 3 that points to the 'Younger phases of the Hongliuhe mélange' indicating an intra-arc ocean that opened between the units of the Gongpoquan composite arc. Following to

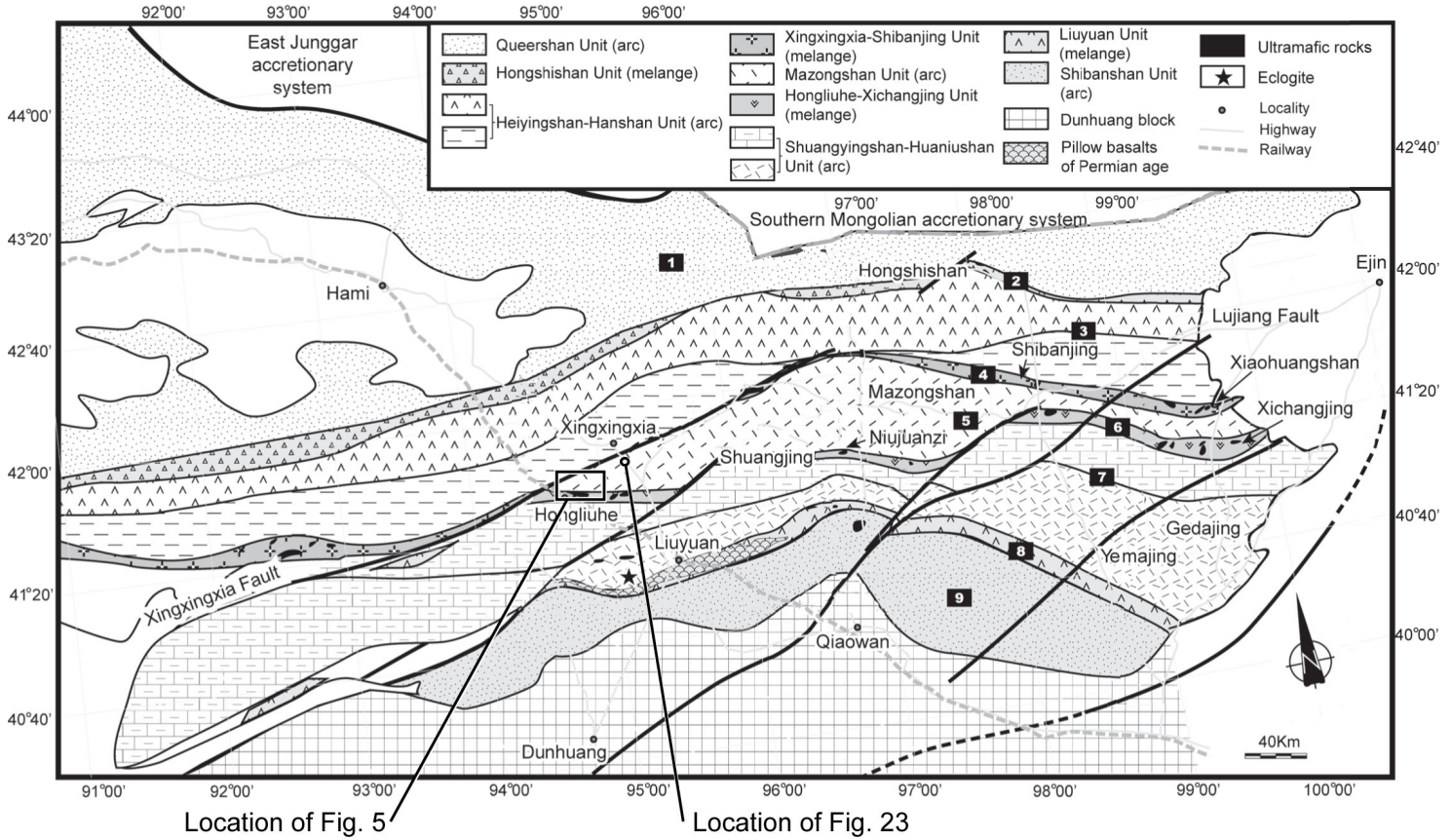

Figure 2: Tectonostratigraphic terrane map of the Beishan orogenic collage. Inset rectangle is the general study area and the location of Figure 4. The inset circle is the location of Figure 22. (Modified from Xiao et al., 2011)

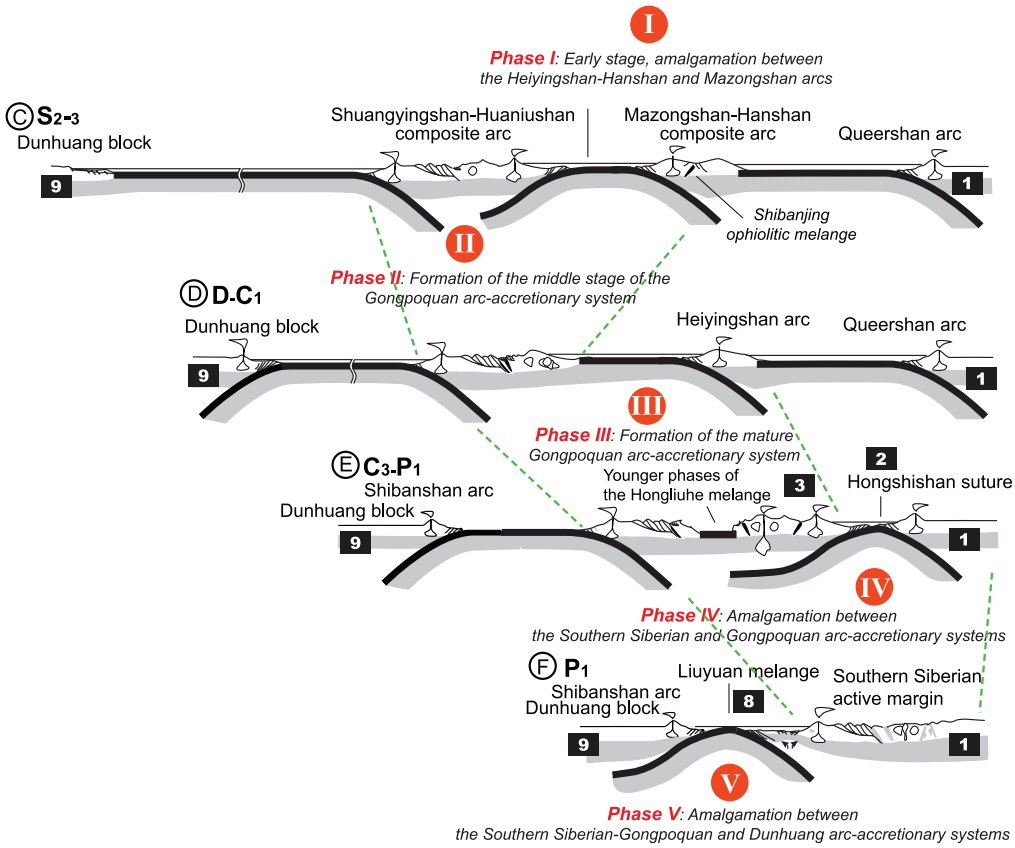

Figure 3: Tectonic model of the development of the Beishan. (Modified from Xiao et al., 2011)

'Phase IV' the Hongliuhe ocean basin has been closed and collision has occurred between the two portions of the Gongpoquan arc-accretionary system. This is the tectonic event that this study indicates is directly related, in accordance with this sole proposed model of Xiao et al. (2011), to the formation of the Hongliuhe Group.

1.5 The Hongliuhe Group

The Hongliuhe (*Red Willow River*) Group is situated directly to the north of the east-west trending Hongliuhe ophiolitic mélange. The Group is in fault contact to the north with metamorphic rocks associated with the Mazongshan arc terrane. The Hongliuhe was elevated to Group status by Li et al. (2006) from Formation, and therefore now has formation divisions outlined by their study. A brief summary of the formations follows according to Li et al. (2006) from the youngest to oldest.

1.5.1 Hongliujing Formation

The Hongliujing (*Red Willow Well*) Formation represents roughly the upper one-quarter of the Group's total thickness. It reflects mainly nearshore oceanic deposition with its lithologies including mostly plagioclase-feldspathic arenites, calcareous siltstones and minor amounts of arkosic arenites and micritic limestones. There are deposits of brownish yellow calcareous boulder conglomerates. The study notes that it is restricted to the central, youngest strata of a large synformal structure. It is noted that its base is a paraconformity with the lower formation.

1.5.2 Luweijing Formation

The Luweijing (*Reed Well*) Formation equals roughly one-half of the Group's total thickness. It is a sequence of rhythmically interbedded feldspathic arenites and siltstones. Siliciclastic mudstone and micritic mudstone are also interbedded but are less voluminous. The lower member contains some strata of polymictic conglomerates and the upper member monomictic granitic boulder conglomerates. The study indicates that the Luweijing contains palynological fossils of a Permian age. It also states that the Luweijing Formation unconformably overlies the Hongliucun Formation beneath it.

1.5.3 Hongliucun Formation

The Hongliucun (*Red Willow Village*) Formation is a thin package of basic and intermediate volcanic rocks with overlying volcaniclastic deposits.

1.5.4 Hexi Formation

The Hexi (*West of the River*) Formation represents roughly one-sixth of the Group's total thickness. It is a fining-upward sequence that starts with a basal monomictic granitoid boulder conglomerate. It changes up-section into a pebble conglomerate, then to a sandstone and to a small amount of carbonate rocks at the top.

1.6 Thesis Outline

This dissertation is organized into four sections, the first being the introduction. The second section introduces this study's analysis of the lithologies associated with the Hongliuhe Group. Structural observations and measurements are reported in the third section in three separate subsections. These outline the faults and shear zones within the area, the folding structures, and a structural cross-section produced from a road-cut outcrop in the Hongliuhe Group that can be seen on the fold-out sheet. The last sections discuss the relevance of the project to the tectonic closing history of the Beishan, how this relates to the evolution of the Central Asian Orogenic Belt, and state the final conclusions for the large and local scale.

2 Lithology and Stratigraphy of the Hongliuhe Group

The Hongliuhe Group has been subdivided by previous workers into distinct formations (Li et al., 2006). This thesis recognizes the characteristics of the formations in the mapped stratigraphy, but has come to different conclusions about their organization. The reasons for this conclusion will be discussed in detail in following sections, but in order to provide the context, this study considers most of the unconformable contacts outlined by Li et al. (2006) to be fault contacts that juxtapose older sections against younger. This consideration severely limits the usability of the formation names, as stratigraphic reconstruction may beg redefinition of the terms.

Generally speaking, this study finds that the lower strata of the Hongliuhe Group are coarser, with considerable sections of conglomerates. The upper sections of the Hongliuhe Group lack extensive conglomerates and are restricted to rocks deposited in nearshore marine depositional settings. This section describes the geology of the portion of the Hongliuhe Group which lies within the mapped area (Fig. 4), which shows a general trend of moderately to steeply north-dipping strata, of mostly sandstone in the south, and conglomerates in the north. The volcanic rocks located within the bounds of the Hongliuhe Group are classified as part of the formation by Li et al. (2006), and are interpreted to be the base of the succession in this work. The excellent exposure and lack of vegetation in the area allow excellent imaging of structure from satellite maps. Bedding and fault traces, visible on satellite maps in many areas, helped with developing traverse plans and understanding the extent of faulting and folding (Fig. 5). The traces were especially useful in picking out the large-scale eye-fold in the Hongliuhe Group that will be referred to in later sections. Figure 5B shows one of the complete elliptical bedding traces of the the eye-fold highlighted in red.

2.1 Bounds of the Hongliuhe Group

The Hongliuhe Group is found north of the Hongliuhe mélange zone as a fault-bounded package of sedimentary rocks unconformably overlying a small package of volcanic rocks. The volcanic rocks, dated with Ar-Ar isotopic methods by previous workers, are considered to be of Late Carboniferous to Early Permian age (Pan et al., 2008). They are fault-bounded at their base, which limits the estimates of their original thicknesses. The Hongliuhe Group, which extends outside the map area along strike, is bounded by faults in the north and south. It also contains several faults within the formation. The Permian strata are spatially limited, being found strictly north of the Hongliuhe mélange zone; there are no deposits linked to the Hongliuhe

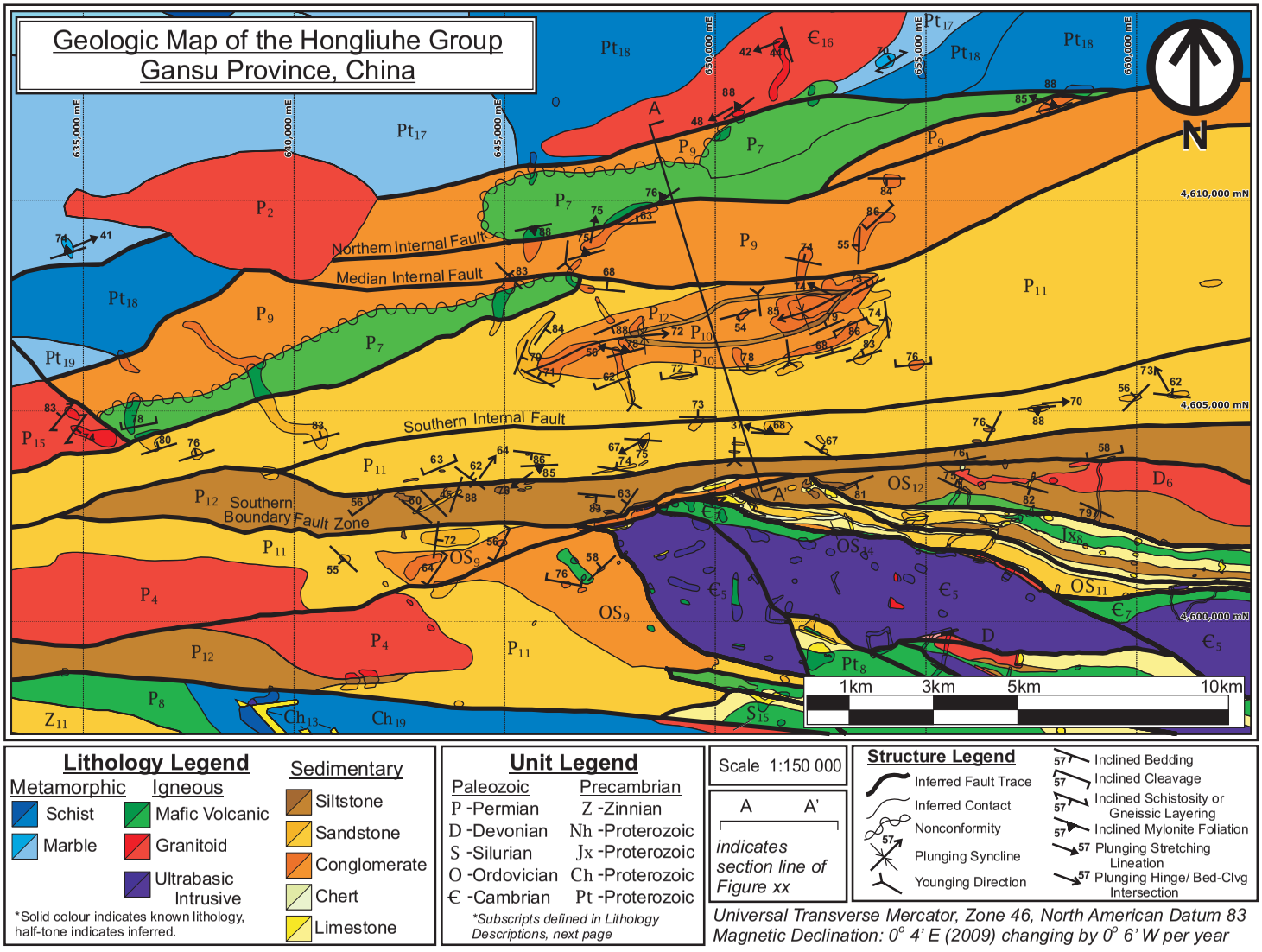
Geologic Map of the Hongliuhe Group
Gansu Province, China
N
635,000 mE
640,000 mE
645,000 mE
650,000 mE
655,000 mE
660,000 mE
4,610,000 mN
4,605,000 mN
4,600,000 mN
Northern Internal Fault
Median Internal Fault
Southern Internal Fault
Southern Boundary Fault Zone
A
A'
1km 3km 5km 10km
Lithology Legend
Metamorphic
Schist
Marble
Igneous
Mafic Volcanic
Granitoid
Ultrabasic Intrusive
*Solid colour indicates known lithology, half-tone indicates inferred.
Sedimentary
Siltstone
Sandstone
Conglomerate
Chert
Limestone
Unit Legend
Paleozoic
P -Permian
D -Devonian
S -Silurian
O -Ordovician
€ -Cambrian
Precambrian
Z -Zinnian
Nh -Proterozoic
Jx -Proterozoic
Ch -Proterozoic
Pt -Proterozoic
*Subscripts defined in Lithology Descriptions, next page
Scale 1:150 000
A A'
indicates section line of Figure xx
Structure Legend
Inferred Fault Trace
Inferred Contact
Nonconformity
Plunging Syncline
Younging Direction
Inclined Bedding
Inclined Cleavage
Inclined Schistosity or Gneissic Layering
Inclined Mylonite Foliation
Plunging Stretching Lineation
Plunging Hinge/ Bed-Clvg Intersection
Universal Transverse Mercator, Zone 46, North American Datum 83
Magnetic Declination: 0° 4' E (2009) changing by 0° 6' W per year

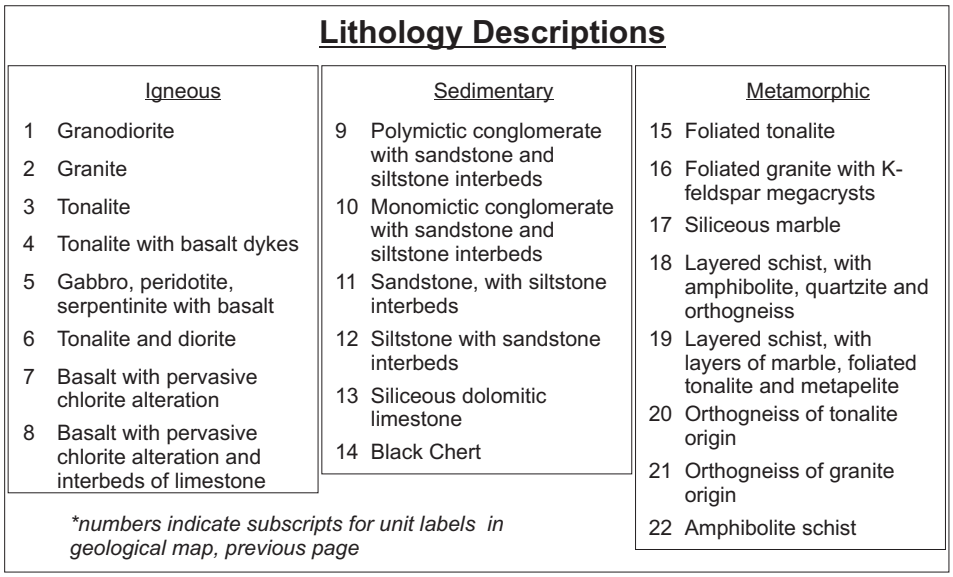

Figure 4: (*Previous page with above unit reference table*) Geologic Map of the Hongliuhe Group showing lithology and structure of the Permian Strata. The time periods assigned to each unit are adopted from Chinese geologic maps.

Group south of the mélange zone (Fig. 2).

The northern boundary of the Hongliuhe Group separates a terrane of more ductile deformed metamorphic rocks, south of the Xingxingxia fault zone (which separates the Mazongshan terrane from the Hanshan terrane, see Figure 2), from the Permian sedimentary rocks, which exhibit little pervasive ductile deformation. The boundary is visible as a sharp contact on satellite photos and is a zone of intense weathering with enough of a topographic depression to channel water flow during wetter times. Though contacts are not observed due to such weathering, deformation is observable at outcrop scale at certain points along the boundary. Mylonite foliations in the metamorphic rocks are typical proximal to the boundary on the North side; these are best seen in rocks with textures that allow for competency contrast amongst textural features, such as the k-feldspar porphyroclasts in granitoid bodies. Deformation on the south side in the Permian rocks is more limited in its forms of plastic deformation, and manifests mostly as deformation of pebbles in conglomerates, stretching to a limited amount. There is a strong implication that there has been later stage brittle faulting that juxtaposed differing degrees of ductile deformation between either side of the fault.

The southern extent of the Hongliuhe Group borders the rocks associated with the Hongliuhe ophiolite and the Hongliuhe mélange zone. The contact where the ophiolite and its contiguous, related sedimentary cover meets the Hongliuhe Group rocks can reasonably be inferred

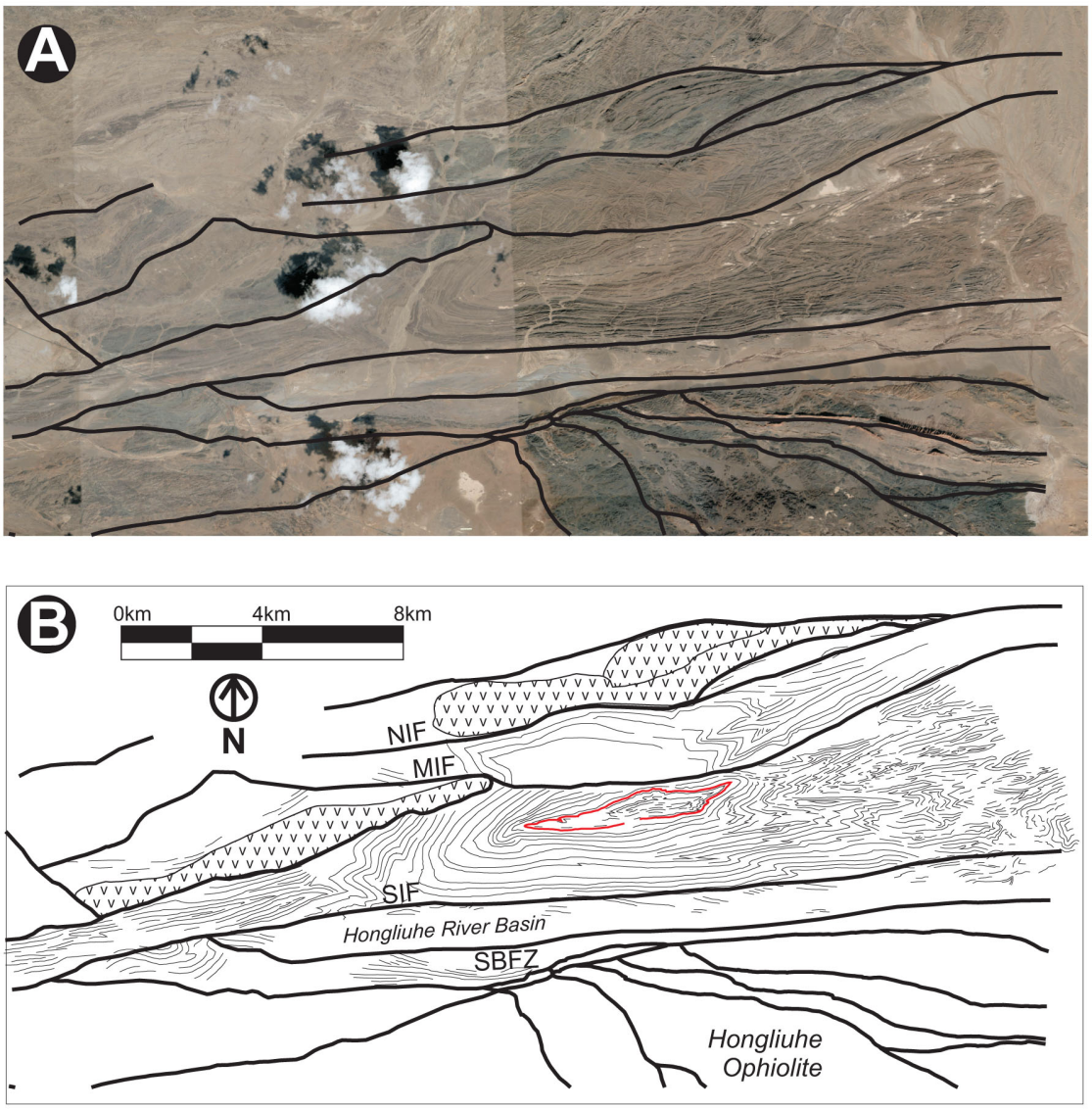

Figure 5: A) Satellite image, from Google Maps, of the field area mapped in Figure 4. Fault traces from Figure 4 have been overlain for illustrative purposes. B) Bedding traces visible on the satellite map traced out to show structure. Relief is minimal in the area. One of the bedding traces associated with the structure referred to in the text as the 'eye-fold' has been highlighted in red. *NIF* Northern Internal Fault, *MIF* Median Internal Fault, *SIF* Southern Internal Fault, *SBF* Southern Boundary Fault.

to be at the sharp lineament, visible from satellite imagery, on the south shore of the (modern day) Hongliuhe (*Red Willow River*). This inference is based on the types of sedimentary rock differing on either side of this fault boundary, their provenance, and the mechanisms, structural styles, and observed degrees of deformation on either side. In the Hongliuhe Group rocks north of this fault boundary, there is some outcrop scale folding and some ductile deformation, which is a different style from that seen in the strata further north. On the south side of this lineament, there is a series of sub-vertically dipping strata interpreted to be the pelagic strata covering the ophiolite. They have experienced different degrees and styles of deformation, both faulting and folding, than the Hongliuhe Group rocks to the north; they contain a series of ductile faults (mylonites) hosted in weaker lithologies, namely carbonate rocks and hydrated basalts intercalated with carbonate material. Given this evidence one can conclude that the Hongliuhe Group lies at the uppermost structural level of the lithologies between the Xingxingxia fault and the Hongliuhe mélange zone, with more deformed and metamorphosed rocks across faults to its north and south.

2.2 Stratigraphic organization of the Hongliuhe Group

A significant conclusion of this paper is that the Hongliuhe Group is a foreland basin deposit, shed from some portion of the Gongpoquan composite arc (Xiao et al., 2011). Foreland basins are a response to a complex interplay between subsidence and collisional orogenic uplift, but the expected pattern of a progressively deepening terrestrial-to-nearshore oceanic basin explains the general fining upwards sequence seen through reconstruction of the mapped stratigraphy (Fig. 6). The reconstructed stratigraphic column's structure and thicknesses are interpreted from the location of the section line in the geologic map (Fig. 4). The main concept behind the reconstruction, the imbrication from faulting that juxtaposed older blocks in the north against younger blocks in the south, is illustrated in the cross-section associated with the section line of the geologic map (Fig. 7). This sedimentary rock sequence was nonconformably deposited on existing volcanic rocks, possibly of oceanic origin (Pan et al., 2008), associated with one of the terranes involved in the collision. The other unconformable contacts of Li et al. (2006) are interpretated as fault zones in this study, the subject of further discussion. The sections that show similar characteristics to the formation descriptions of Li et al. (2006) are noted in the stratigraphic reconstruction with the respective formation names (Fig. 6).

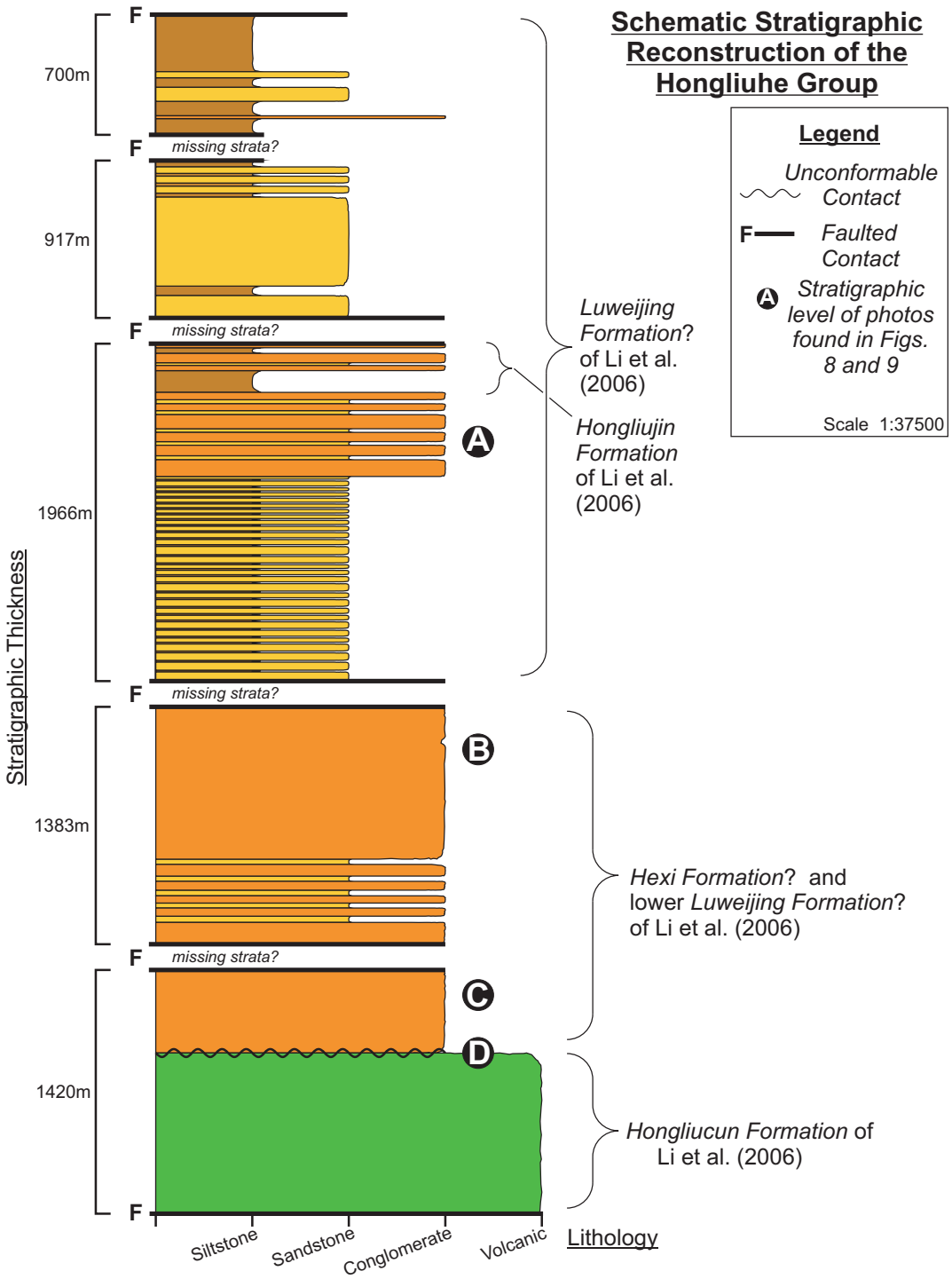

Figure 6: Stratigraphic column of the Hongliuhe Group reconstructed from interpretation of geologic structure. The column's structure and thicknesses are interpreted from the location of the section line in Fig. 4, and its corresponding cross section in Fig. 7. The marked letters show the stratigraphic levels of the respective conglomerates pictured in Figures 8 and 9.

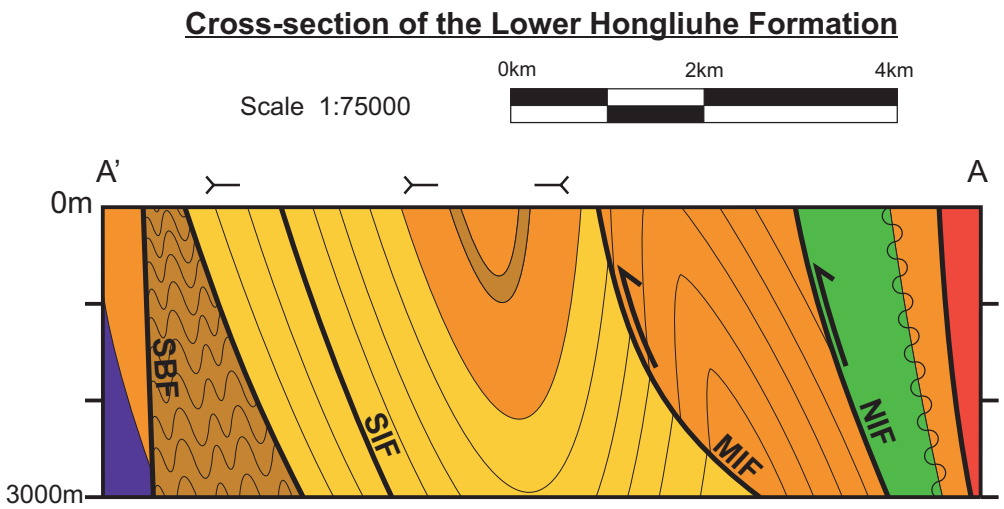

Figure 7: Schematic cross-section of the Hongliuhe Group; section line is marked in Figure 4. *NIF* Northern Internal Fault, *MIF* Median Internal Fault, *SIF* Southern Internal Fault, *SBF* Southern Boundary Fault.

2.3 Sedimentary Petrology

Conglomerates in the Hongliuhe Group show an evolution associated with the progression of unroofing from collisional orogenic uplift and erosion. The younger, upper sections of the Hongliuhe Group contain monomictic conglomerates of mostly unstrained tonalitic granitoids and a small fraction of smaller volcanic clasts (Fig. 8A). The granitoid clasts are sub-angular to sub-rounded, ranging from cobble sized up to large boulders (1-3 m diameter). The clast-size distribution is poorly sorted, and the lithology ranges from clast-supported to matrix-supported (Fig. 11B). Mid-section, some conglomeratic strata contain brownish-yellow siliceous limestone boulders. These deposits range from clast-supported to matrix-supported as well (Fig. 8B). In the lower strata the conglomerates are polymictic and include a very heterogeneous mixture of angular to subrounded boulders and cobbles of gneiss, schist, strained and (rare) unstrained granitoids, marble, limestone and other sedimentary rocks (Figs. 9 C and 10 E–F). These are the general lithologies that make up the Hanshan/Mazongshan composite arc, all of which can reasonably be expected to have been subaerially exposed during the arc's prolonged history.

Sandstone lithologies are commonly mature, grain-supported and well-sorted with grain sizes of 1-2 mm. Weathered outcrop colours range from blue-grey to brown (Figs. 11A and 12C–D). Fresh surfaces are grey to grey-blue. Most samples are composed of almost entirely

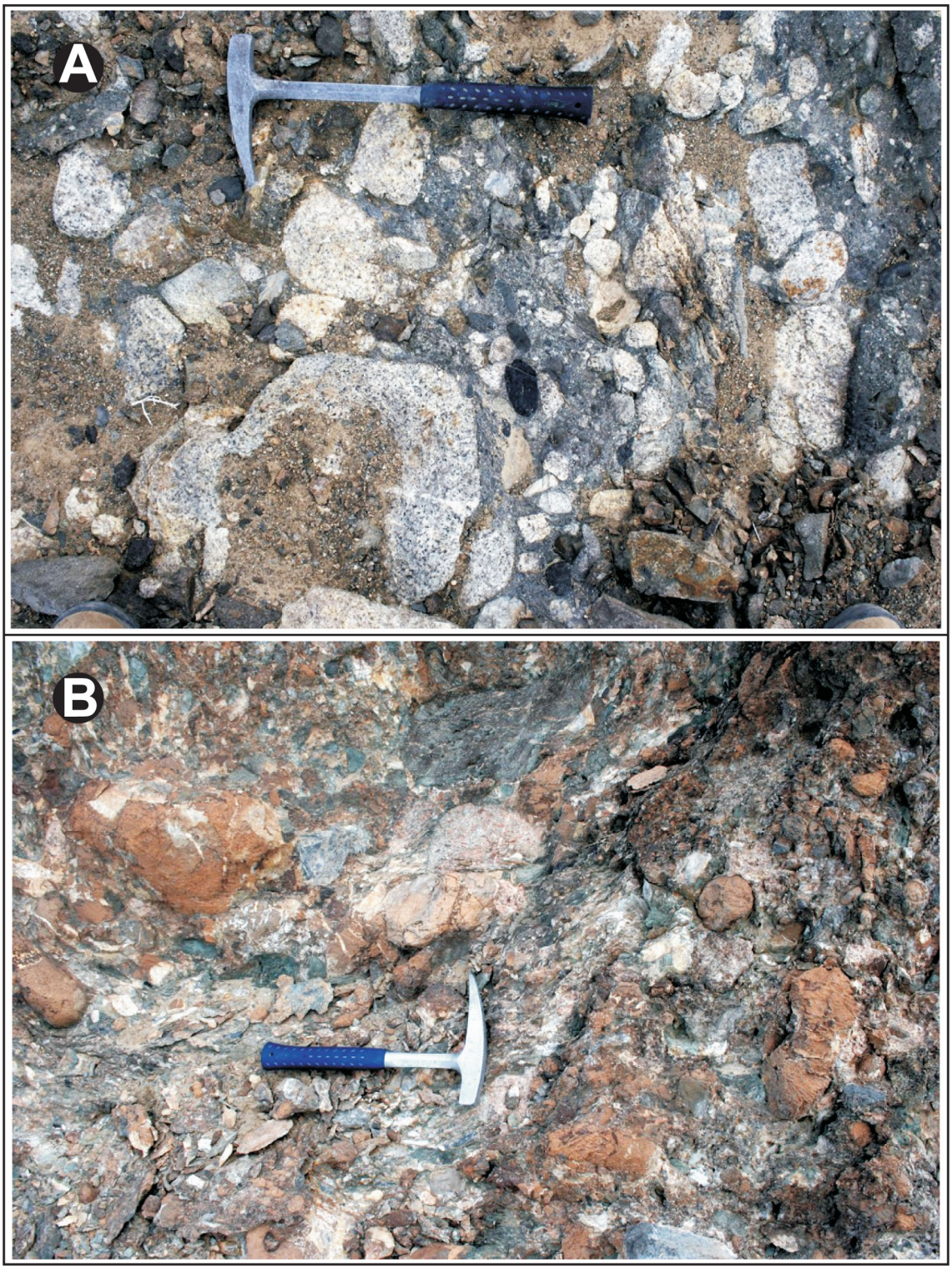

Figure 8: A) Conglomerate consisting of granitoid boulders and volcanic cobbles. B) Conglomerate consisting of limestone boulders and siltstone cobbles. *The stratigraphic levels at which these conglomerates are found are marked in Figure 6.*

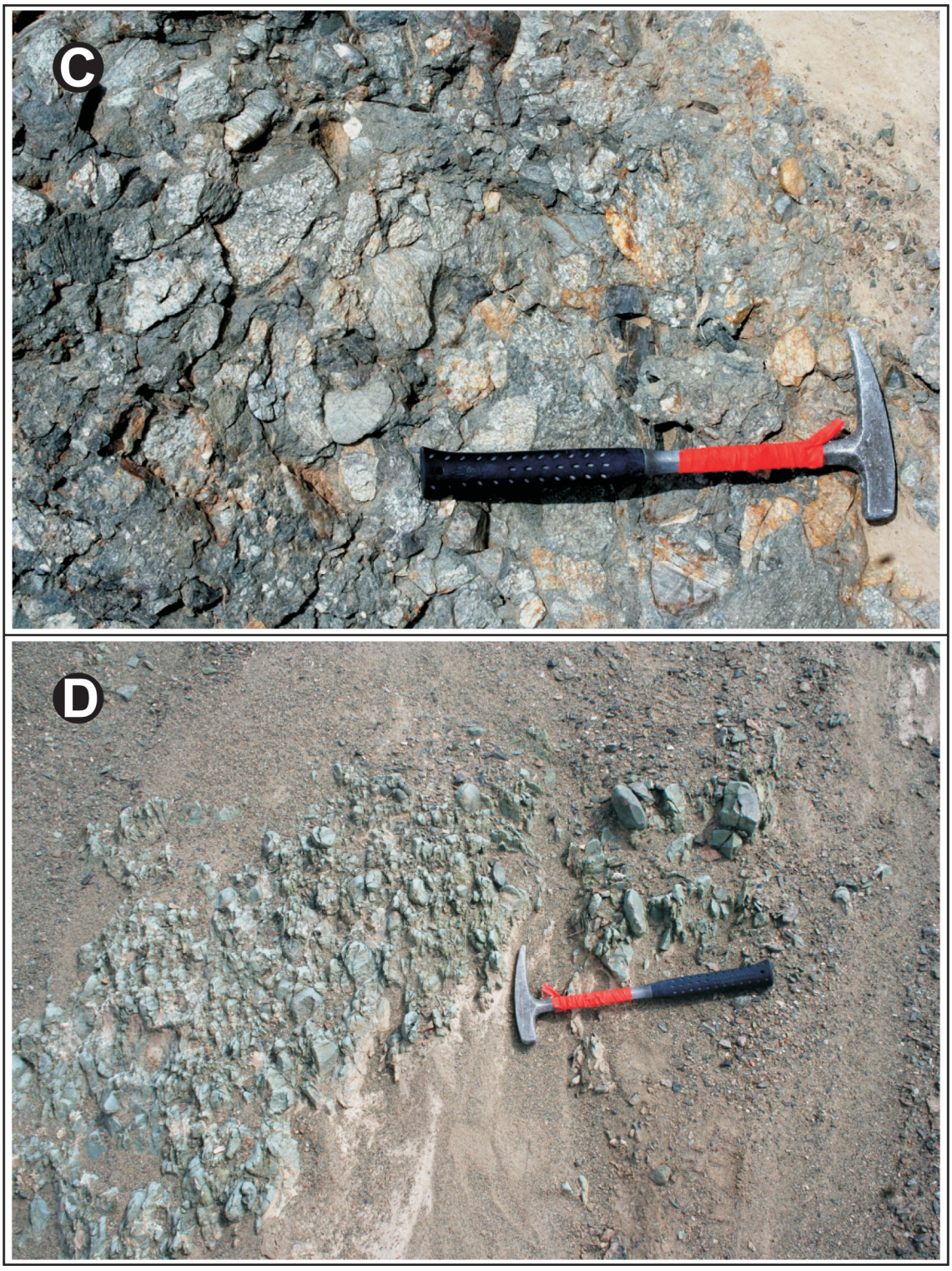

Figure 9: C) Conglomerate consisting of gneiss, schist, granitoid, chert, sandstone, siltstone, and mylonite clasts. D) Evidence of an unconformity, a conglomeratic bed consisting of clasts and matrix of the volcanic unit structurally beneath the sedimentary unit. This shows that the volcanic unit existed prior to sedimentation, allowing it to be sediment source itself. *The stratigraphic levels at which these conglomerates are found are marked in Figure 6.*

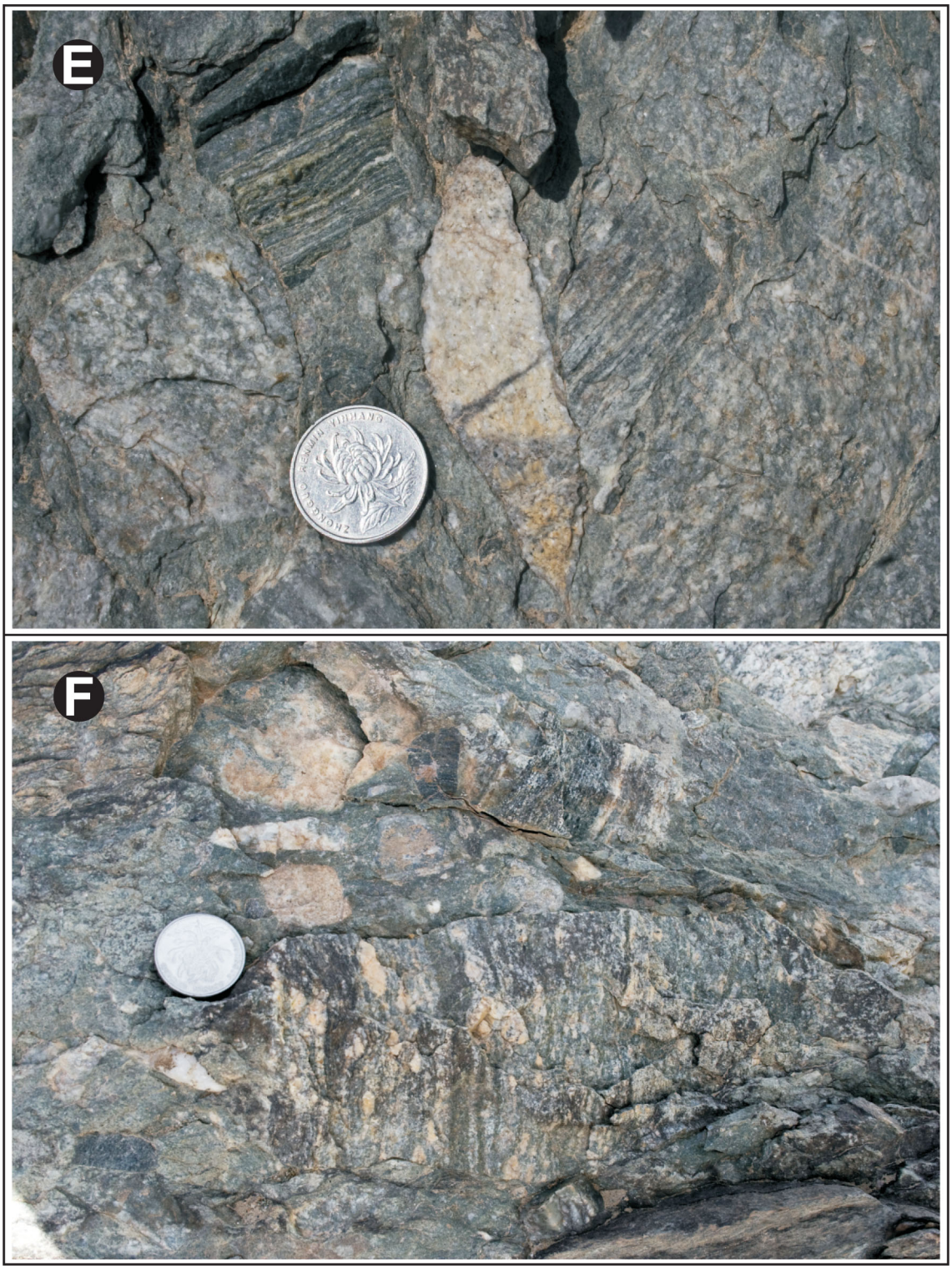

Figure 10: E) Close-up of clasts in the same outcrop as from Figure 9C. Clasts pictured include granitoids, marble, and schist. F) Close-up of clasts in the same outcrop as from Figure 9C. Clast shown is a gneiss.

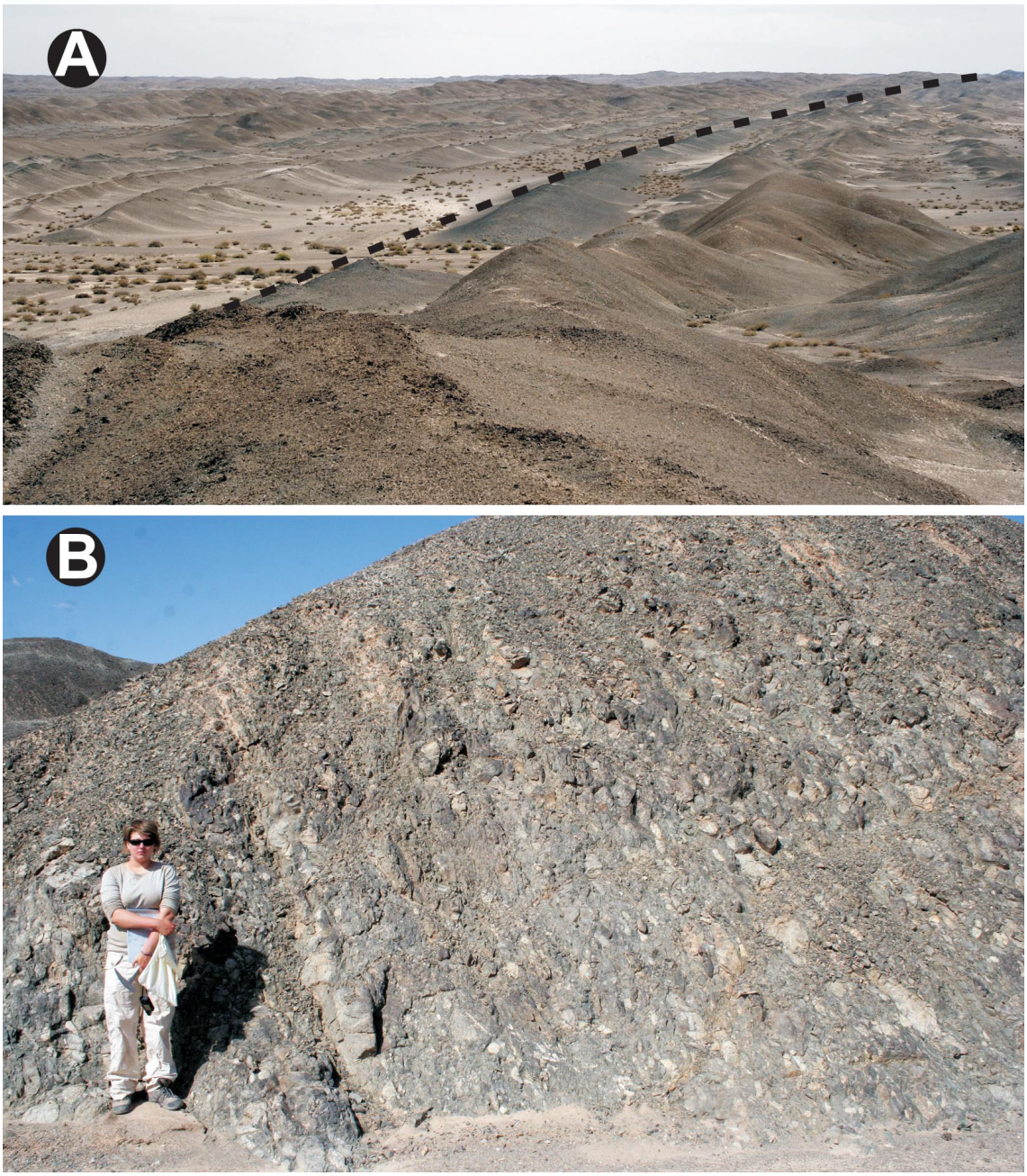

Figure 11: Photographs of outcrop in the Lower Hongliuhe Group: A) Gently curving strata traces *(example trace marked with dashed line)* looking west towards the western hinge of the eye-fold, from the near the center. The hills represent more competent sandstone beds and the weathered areas between are interbedded siltstones. B) Typical outcrop of more indurated mono-mictic conglomerate.

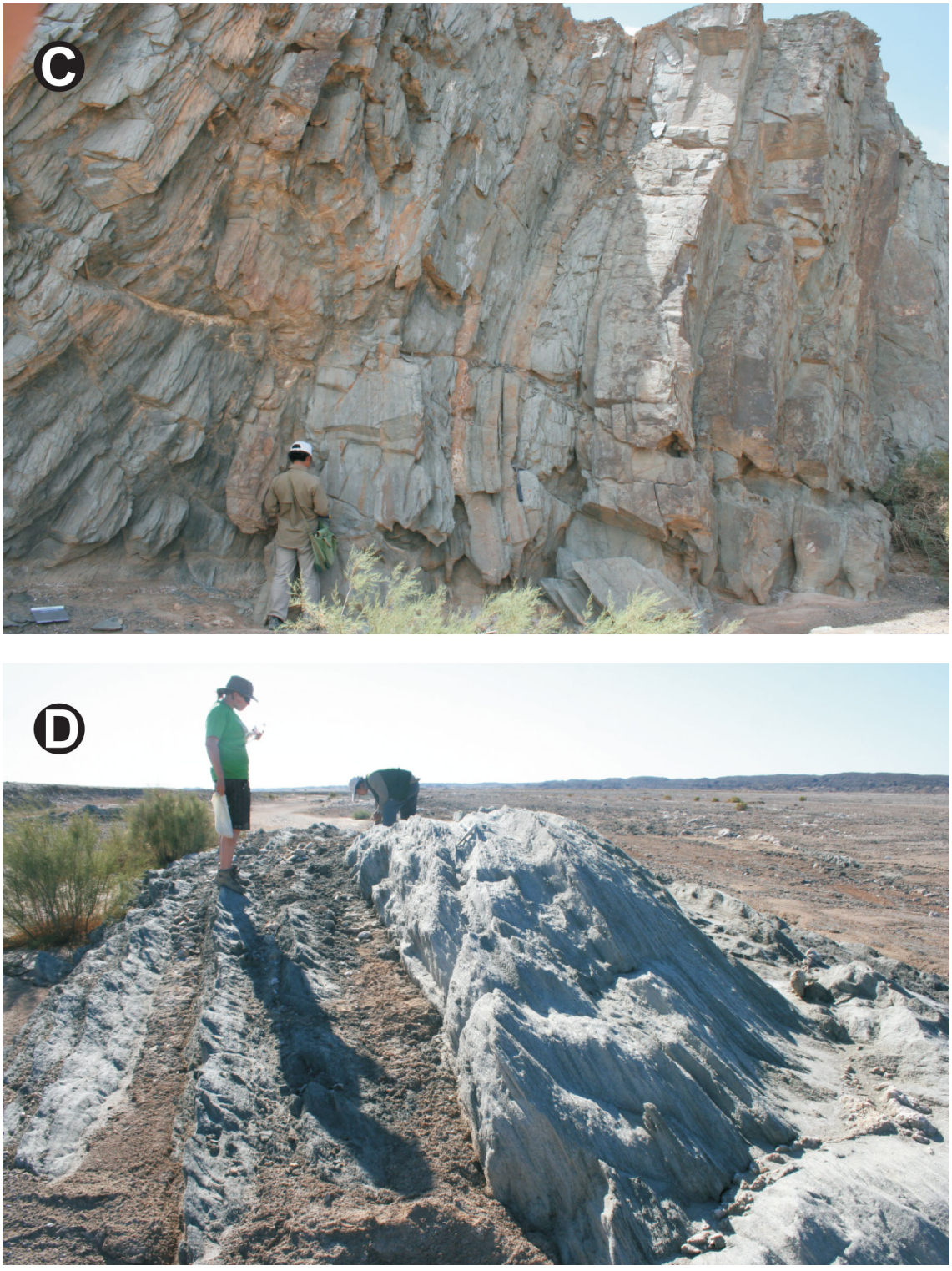

Figure 12: Photographs of outcrop in the Lower Hongliuhe Group: C) Sub-vertically dipping strata towards the southern end of the map area, at the edge of the (modern day) Hongliuhe River basin. Lithology seen is sandstone with small interbeds of siltstone. D) Cross-bedded sandstone outcrop in the Hongliuhe River basin.

sub-angular to sub-rounded quartz grains, with occasional plagioclase grains (less than 2 or 3%) which are sometimes sericitzed. K-feldspar grains and carbonate grains are observed in accessory amounts. Mafic lithic grains are present in variable amounts, from none to roughly 5%. Where present, they are appear as clasts of fine-grained chlorite-altered volcanic material. The sandstones are lithified with a matrix consisting of fine oxide minerals, carbonate and/or sericite, usually less than 15% by volume, but ranging up to rare samples with approximately 40% matrix. Some quartz grains show undulose extinction in thin section but there is no significant level of homogeneous strain throughout the formation. There is also a small percentage of microscopic muscovite grains, occasionally clustered, overprinting the matrix. Bedding can be massive, but is also commonly interbedded with siltstone. In such a case, bed thicknesses range from approximately 30 cm to 3 m, and overall percentage of sandstone interbedding is variable unit to unit.

Siltstone outcrops vary with dark green, dark brown, brown-red and grey weathered outcrop colours (Fig. 12). Fresh surfaces are commonly brown to grey in colour. Grain sizes range from mud particles to sand grains, with the distribution centered around silt size. As with the sandstones, muscovite is a common replacement mineral, with sufficient abundance to give the rocks a slight sheen.

2.3.1 Younging directions

Important in the interpretation of the structural juxtaposition of all these fault bound blocks of sedimentary rocks are younging indicators. The younging indicators found consistently show northward-younging of all north-dipping strata (Fig. 13 A, C–F). The exception to the northward-younging trend is within the north limb of the synclinal fold that produced the eye-fold; the northern limb youngs south, as expected (Fig. 13B). This consistent trend of northward-younging on north-dipping strata is important as it precludes the possibility of the area being a large, overturned nappe. Younging indicators found include cross-bedding, flame structures and other loading features, and graded bedding.

2.4 Petrology and Primary Stucture of the Underlying Volcanic Rocks

Within the mapped bounds of the Hongliuhe Group exist two distinct bodies of basaltic volcanic rock. These two are interpreted to be one body that has been structurally dismembered and faulted to show a repetition of lithologies seen in the regional map (Fig. 4). These volcanic rocks are basic in composition and vary in degrees of alteration and deformation. The por-

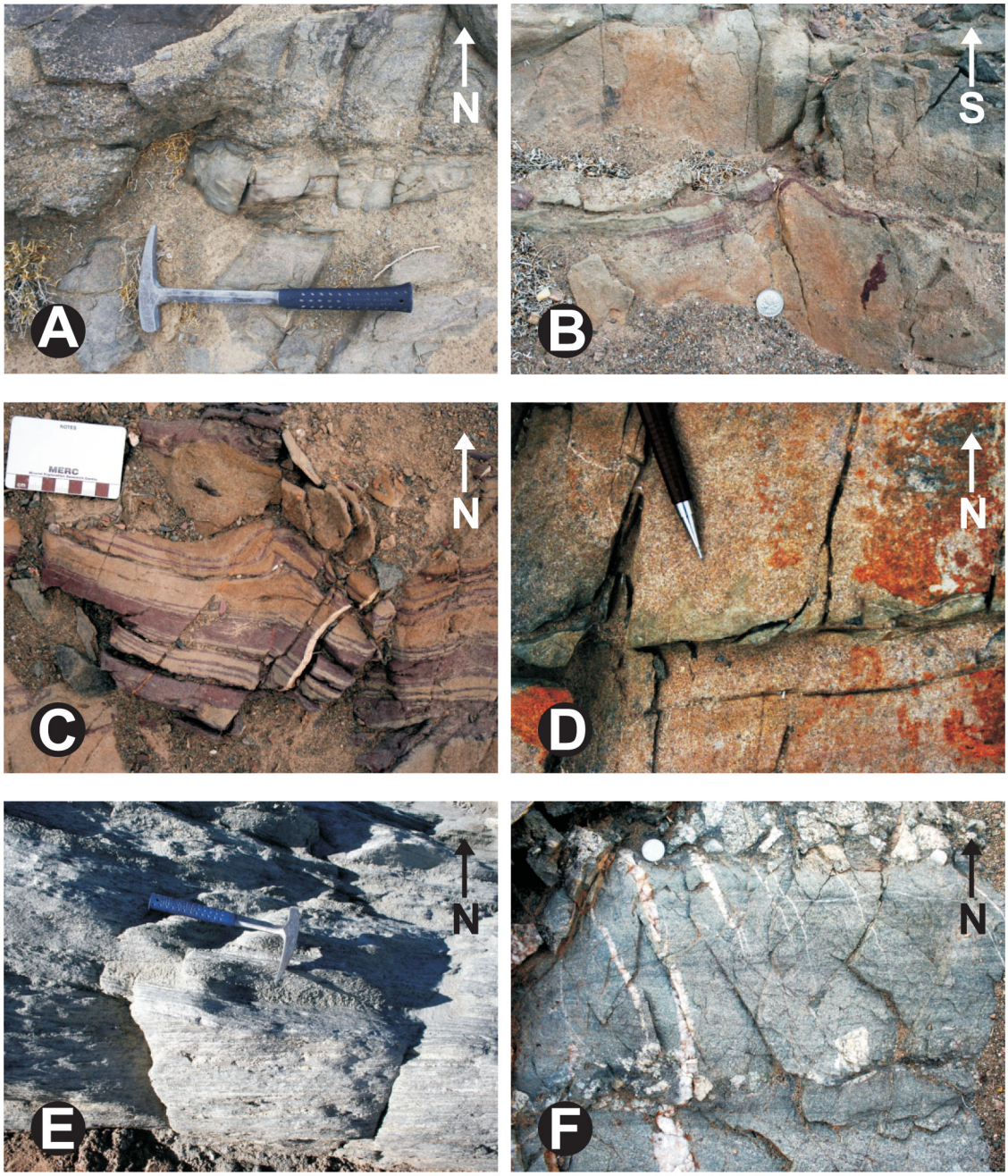

Figure 13: Younging indicators: A) Flame structure of sandstone pushed into a pebbly bed. B) Flame structure of purple mudstone layer pushed up into a sandstone layer. C) Well developed flame structure consisting of layers of mudstone and sandstone. D) Flame structures of green siltstone pushed up into sandstone. E) Cross-bedding in sandstone. F) Cross-bedding in sandstone.

tions in the northeast that are faulted directly against the metamorphic rocks to their north are less deformed and less altered, compared to most everywhere else. In the southern and western portions of the volcanic units the alteration is pervasive, and deformation is sporadic but relatively intense. Alteration is typical of a mafic rock, with extensive amounts of chloritization and epidotization. The outcrops range in colour from light green, to dark green and dark grey to black. Fresh surfaces range from green to grey. The rocks commonly consist of fine sub-millimeter crystals with a glassy matrix. Phenocrysts of plagioclase and pyroxenes, millimeter to sub-millimeter sized themselves, are observable in some locations. Plagioclase phenocrysts, when present, are euhedral to subhedral and commonly altered to sericite. Chlorite is a common secondary mineral, a product of alteration of the groundmass. Some sample locations exhibit amygdules of calcite, up to 5 mm in diameter.

Some outcrops contain what look like clasts of unaltered material (Fig. 14A). These are probably not clasts, *per se*, but are interpreted to be lenses of less deformed and altered material. The combination of deformation and alteration creates a positive feedback loop, with deformation enhancing alteration and vice versa. In a fine grained, competent basalt strain would have initially localized in narrow bands, thus preserving such undeformed patches. An opposing, or alternate, concept is that it is a primary volcanic rock with inclusions of country rock or magma of different composition and texture. The former assumed hypothesis is supported by features of the outcrop and of the lenses of original material: the contact between the lens and matrix is diffuse, there is evidence of boudinaging, of minor intra-lens stretching of amygdules, and the general alignment of the lenses into a foliation and lineation. Boudinaging implies stretching deformation and a competency contrast between the altered fine material in localized strain zones and the original rock between. The presence of both boudinaging and alignment at a large scale suggests that secondary processes (alteration and deformation) were involved, and not just imbrication of clasts from volcanic deposition and flow. This is also supported by the observation that the material forming the matrix between the lenses is devoid of any primary volcanic textures.

The volcanic packages are bound by faults on their southern limits where they contact the Hongliuhe Group, and are in contact with Hongliuhe Group conglomeratic units to the north. The northern contacts, are inferred to be unconformable, or more specifically, disconformable. Within the polymictic conglomerate unit immediately north of the volcanic package, an approximately 5 m thick bed of conglomerate that is composed entirely, both rounded-cobble clasts and matrix, of altered volcanic material, lies within tens of meters of the basal contact. The volcanic material that comprises the clasts and matrix is visually identical to the altered

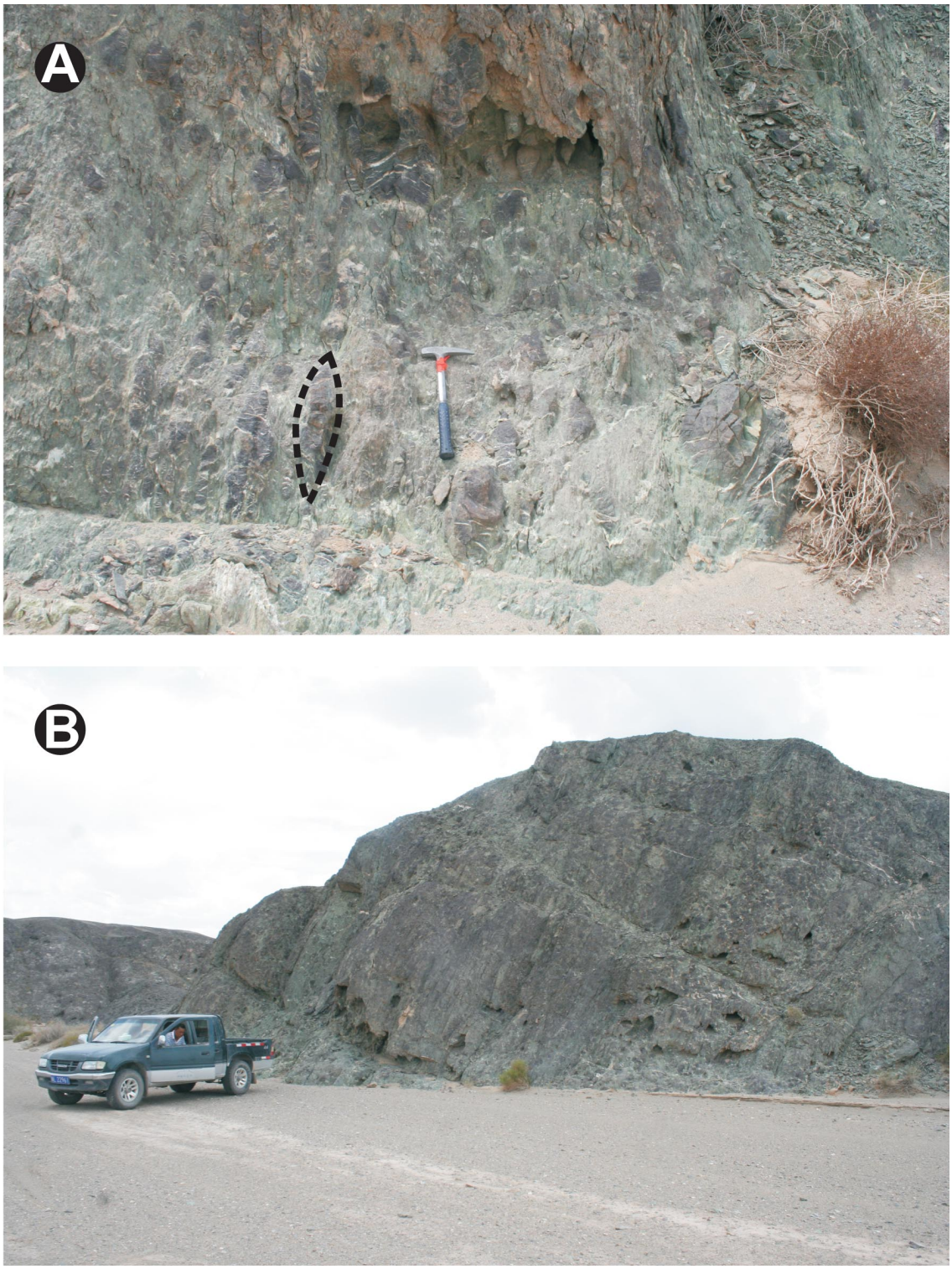

Figure 14: Photographs of outcrops of volcanic rocks that underly the Hongliuhe Group: A) Black lenses of primary volcanic in a matrix of green, fine-grained, deformed, altered volcanic material. *One lens is outlined with dashed line for example, to the left of the hammer.* B) Deformed volcanic proximal to the Northern Internal Fault. This outcrop contains hollows that expose the lineation in the deformed unit.

portions of the volcanic packages (Fig. 9D). Composed of rounded cobbles up to 15 cm in diameter, the bed is poorly sorted and matrix-supported with a very fine matrix. It is traceable for approximately one hundred meters, parallel to the contact. These observations imply that the volcanic rocks existed prior to the deposition of the conglomerate, and were not erupted through it or into it. This disconformity is interpreted to be the base of the formation when taken with consideration of the structural juxtaposition of older units against younger from north to south.

3 Structure in the Hongliuhe Group

The recognition of faulting in the formation has proven to be the key structural aspect for elucidating tectonic and stratigraphic interpretation. With excellent outcrop exposure both fault and bedding lineaments are traceable throughout the breadth of the area approached in this study. This has been a boon to the research as it shows the direct relations between faulting and folding. Visible on satellite imagery are not only the fault lineaments but also various large- and meso-scale folds, eye-folds and apparent fold interference patterns (Fig. 5). The fold interference patterns suggest one of two alternatives: multiple deformation events or a prolonged significant shortening and thickening of the sedimentary package through localized fault zones and folding within the bound blocks between them. Supporting the latter idea are the observed repetition of sections of strata, implying thrust stacking. This study also shows how, in the upper sections of the Hongliuhe Group, a complicated fold-thrust belt collection of low-angle fault displacements and shear-style folding accommodated shortening, with exposures recorded and mapped in a road-cut near the town of Xingxingxia.

The mapped part of the formation exists as numerous packages of strata separated by faults (Figs. 4 and 7). It shows that the Hongliuhe Group is punctuated by intermittent zones of brittle/ductile deformation that verge steeply south. The shear zones define contacts between units and separate discrete packages of sedimentary strata of the Hongliuhe Group. The mechanisms of deformation at the grain scale are observable, and the scale of stretching/flattening is finite and measurable though it is unknown exactly how much displacement occurred across such faults. This uncertainty has restricted the ability to exactly reconstruct stratigraphy: one cannot be sure if there are missing strata between faulted blocks, or conversely, if there are repetitions of sequences unnoticed due to surficial weathering and erosion of sections of the outcropping strata. Most of the faults have experienced dominantly dip-slip motion, though evidence of some lateral movement was recorded.

3.1 Shear Zones

There are three major shear zones within the package of rocks associated with the Hongliuhe Group. Generally, the shear zones involved verge steeply south and experienced mainly dip-slip displacement with minor strike-slip movement more pronounced in the southern faults. These zones exhibit fabrics associated with simple shear deformation though may involve some pure shear flattening. For the purposes of this thesis they will be given functional names, starting from north to south along the cross section line in the geologic map (Figs. 4 and 7): the

'Northern Internal Fault' is the northernmost fault within the formation (inside the mapped area); the 'Median Internal Fault' and 'Southern Internal Fault' border the eye-fold (Fig. 5) on the north and south, respectively; and the 'Southern Boundary Fault' names the fault that borders the ophiolite package to the south. One noted feature of the Median Internal Fault is that, if its trace is followed along strike to the west of the section line it branches, the southern branch is shown to contact the south side of a volcanic unit. This contact is interpreted to be the base of a repetition of the lithologies north of the Northern Internal Fault, faulted to its current position.

This nomenclature does not include the shear zone bordering the formation to the north, as a high degree of deformation is observed only in the hangingwall, not in the Hongliuhe Group. This effect is considered the result of further brittle faulting along the same structure juxtaposing more deformed, deeper, older rocks in the north against the Permian sedimentary rocks in the South.

3.1.1 The Northern Internal Fault

The Northern Internal Fault (NIF) juxtaposes the base of the volcanic unit as the hangingwall against the polymictic conglomerates of the lower strata of the section, the footwall. The observed fault contact shows a sharp change in lithology girdled by zones of intense deformation on the scale of tens to low hundreds of meters in both directions (away from the strike trace) (Fig. 15A–B). This fault shows similar degrees of strain on either side of the contact. Figure 15A shows the contact between the volcanic unit, the hanging wall, and the Permian conglomerate, the footwall, and similar degrees of ductile deformation in both lithologies. The effects of pressure solution can be observed in the reshaping conglomeratic clasts, with harder clasts impinging on softer. Clasts are stretched and flattened, creating the visible foliation, its associated cleavage, and a strong lineation. Though the volcanic rock shares a similar degree and style of deformation it lacks a strong foliation, a product of its inherent homogeneity and fine grained texture. As noted in the volcanic unit's description, the lenses of less altered material are aligned, which is a lineation structure difficult to gauge and measure. Figure 16C shows one location, a small weathered hollow in the outcrop pictured in Figure 14B where the ellipsoidal lenses are exposed. The only foliation, a strong cleavage, found in the volcanic unit is hosted in limited volcaniclastic layers within the package (Fig. 16D).

Structural samples taken (Figs. 17A–C and 18) show limited effects of grain-scale ductile deformation mechanisms in the conglomerate of the footwall block. Hand samples depicted

Figure 15: Outcrop pictures of the Northern Internal shear zone: A) Contact between the conglomerate and the volcanic unit along the northern fault zone. B) Foliation developed in the conglomerate within the shear zone boundary of the northern fault zone.

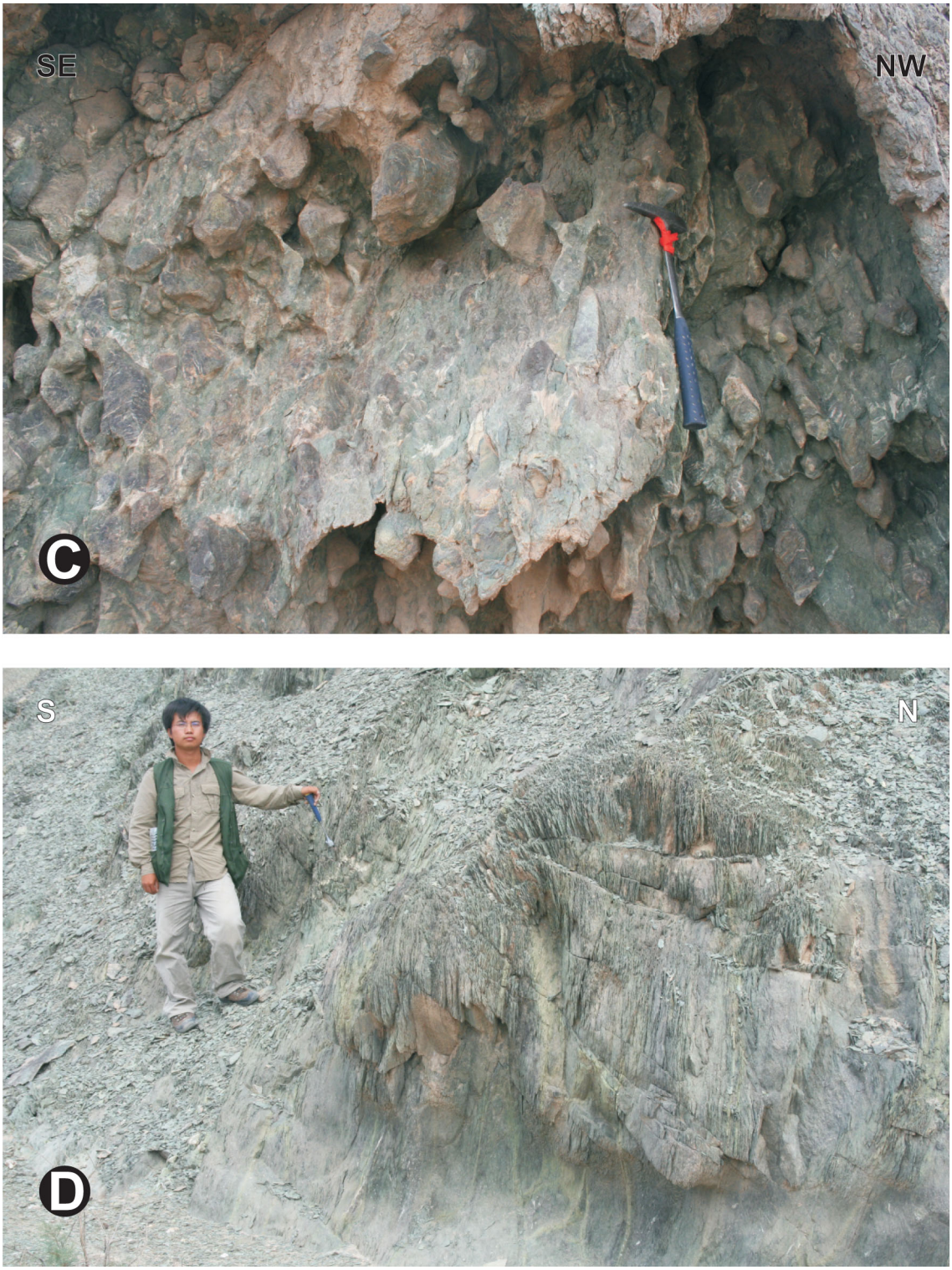

Figure 16: Outcrop pictures of the Northern Internal shear zone hangingwall: C) Lenses of primary volcanic material forming the lineation in the fault zone. D) Foliation developed in fine-grained volcaniclastic rocks within the volcanic package.

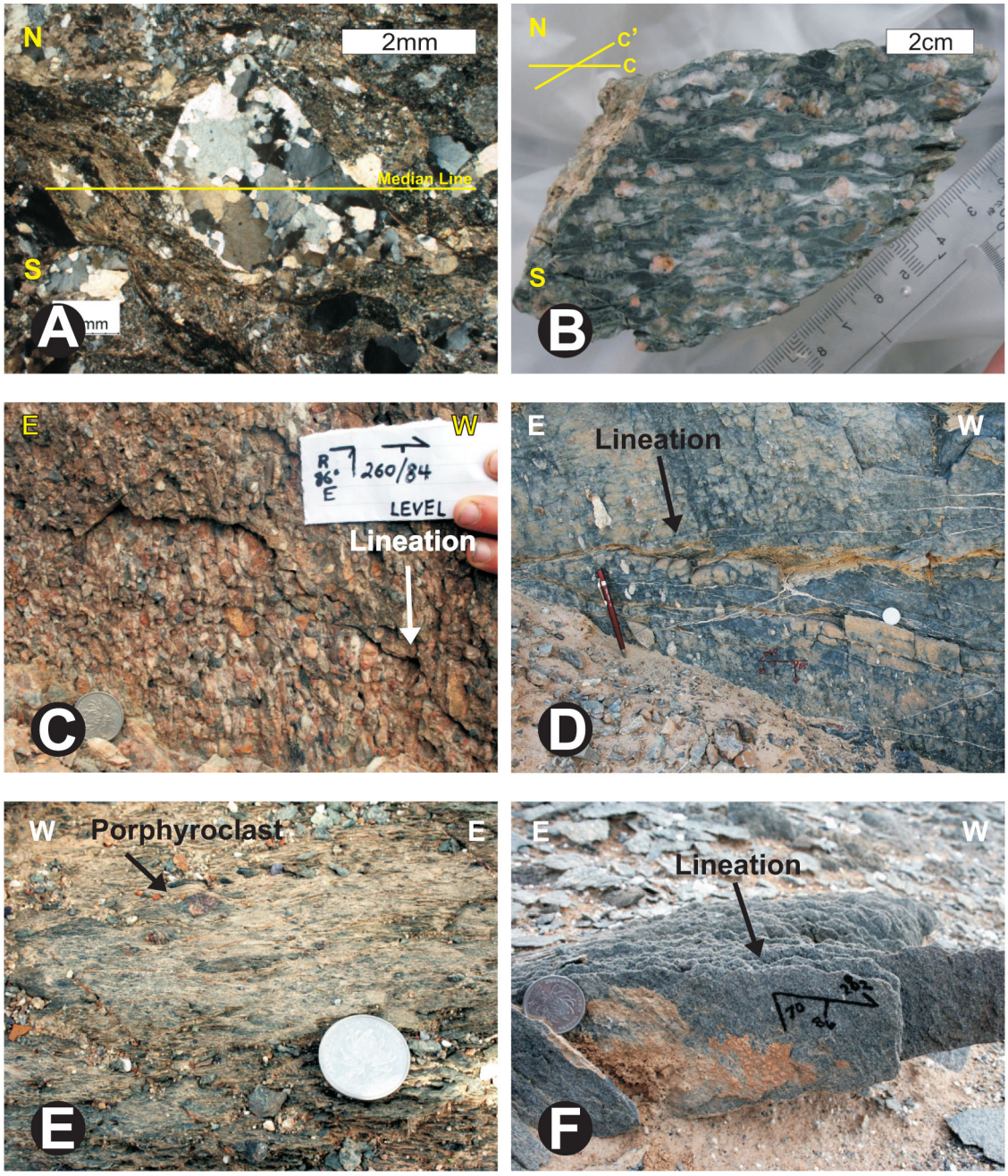

Figure 17: Kinematic indicators of ductile faulting: A) Mantled cluster of dynamically recrystallized quartz grains, indicating north-over-south movement along the steeply north-dipping northern fault zone. B) C' fabric in an altered conglomerate indicating north-over-south movement along the steeply north-dipping northern fault zone. C) Ductile stretching lineation associated with the northern fault zone (and above two samples). D) Stretching lineation in outcrop located along the lengthwise axis of the sheath fold. E) Symmetrically mantled porphyroblast from the southern fault zone; no kinematic indicators were found. F) Stretching lineation associated with the southern fault zone.

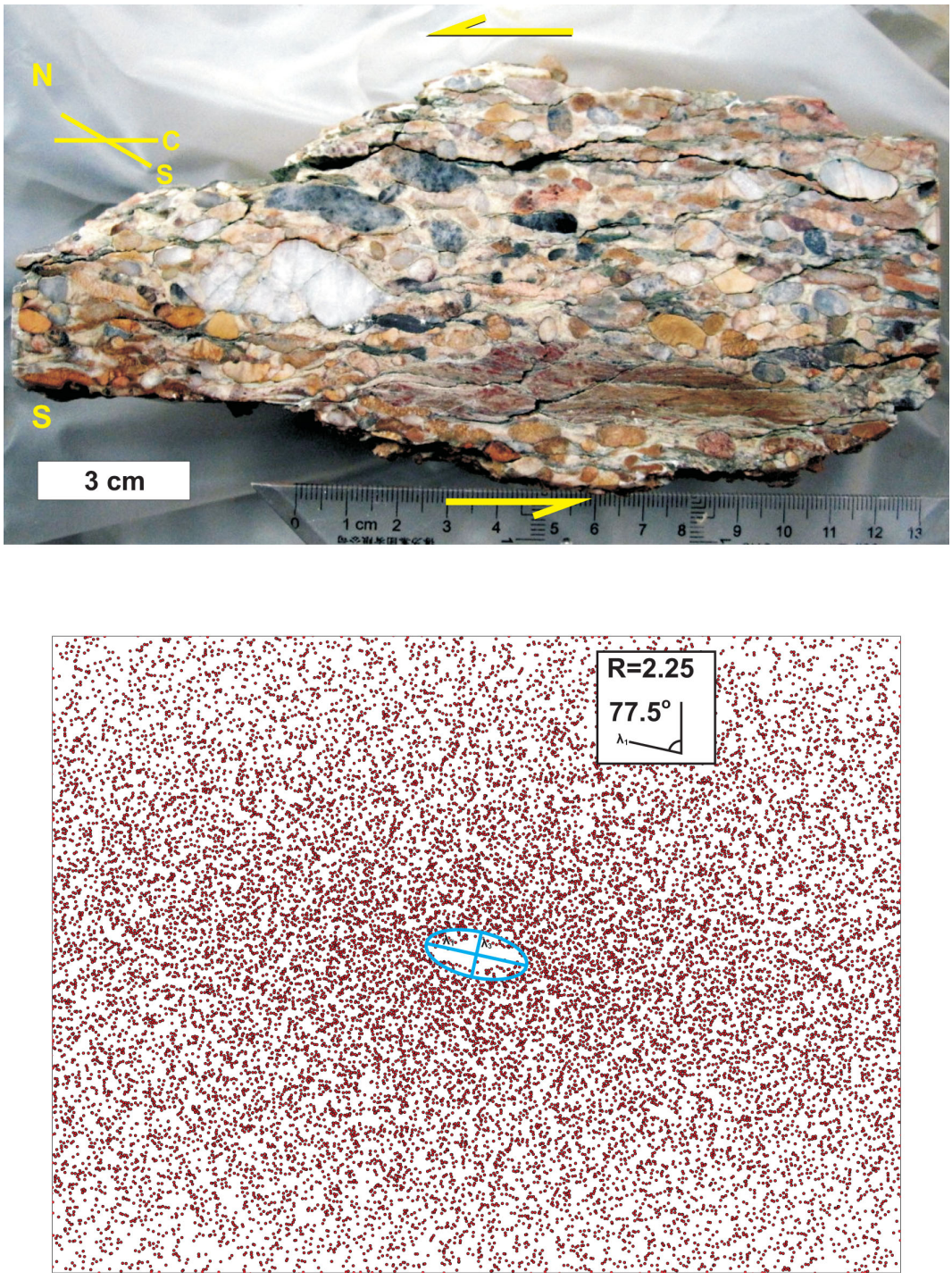

Figure 18: Strain analysis of a deformed conglomerate: A) Deformed conglomerate sample with the cut face in the kinematic plane. B) Fry plot showing the strain ellipse of the above sample.

(Fig. 17B) were sampled near the shear zone contact and from a location approximately 150 m south of the volcanic/sedimentary contact (Fig. 17A, C); the effects of shearing in the rock gradually dissipate southward within 30 m of this location. Closest to the center of the shear zone, and the contact with the volcanics, the pebble conglomerate sample in Figure 17B shows extensive chloritization in the matrix associated with mineral laden fluid circulation proximal to the altered volcanics on the other side of the shear zone. This chloritization has provided mineralogy conducive to the formation of the $C - C'$ fabrics visible in such a cut face showing the kinematic plane. Strain shadows of silica are noticeable winging the more competent porphyroclasts. Chlorite infills tension fractures in the more competent porphyroclasts depicting both the brittle-ductile nature of the deformation and the extensional characteristics of the C' fabric in such a stress regime. The mantled porphyroclast in this series (Fig. 17A) shows minor bulging recrystallization in the porphyroclast of quartz grains and strain shadows of carbonate and oxide materials. This type of recrystallization limits the temperature and pressure of deformation to equate to moderate depths associated with subduction zones, around the brittle-ductile transition zone. A deformed conglomerate sample (Fig. 18) taken from this shear zone exhibits impingement of some clasts into others, evidence of stress induced solution transfer. Some grains also have mantles of calcite or quartz. Figure 17C shows the foliation surface at a similar proximity to the shear zone boundary and shows how pebbles in the conglomerate are still recognizable though stretched to create the lineation. Figure 18, a Fry plot of the centers of the deformed pebbles in the shown sample provides a measure of the degree of deformation from faulting (Fry, 1979a,b; Crespi, 1986; Erslev, 1988; Dunne et al., 1990; Treagus and Treagus, 2002) : the aspect ratio of the strain ellipse is approximately 2.25:1 for $S_1 : S_3$. The angled orientation of the strain ellipse supports the supposition that this sample has been sinistrally sheared (in the provided view, the kinematic plane, it corresponds to north-over-south dip-slip movement).

3.1.1.1 *Structural Data and Kinematics of the NIF*

The Northern Internal Fault dips moderately to steeply north and has a down-dip pitching stretching lineation (Fig 19A) expressed in the conglomerates of the footwall block. Kinematic indicators shown in deformed conglomerates all point towards north-over-south motion across the fault. The sinistrally mantled porphyroclst of Figure 17 A, the C' fabric in Figure 17B and the sheared conglomerate used for the fry diagram (Fig. 18) all consistently correspond to north-over-south dip-slip motion along the fault. The lineations in the footwall conglomerates (Fig. 17C) are entirely down dip, but a small amount of data points measured from the volcanic rocks of the hangingwall show a different trend (Fig. 19B). These lineations, plunging

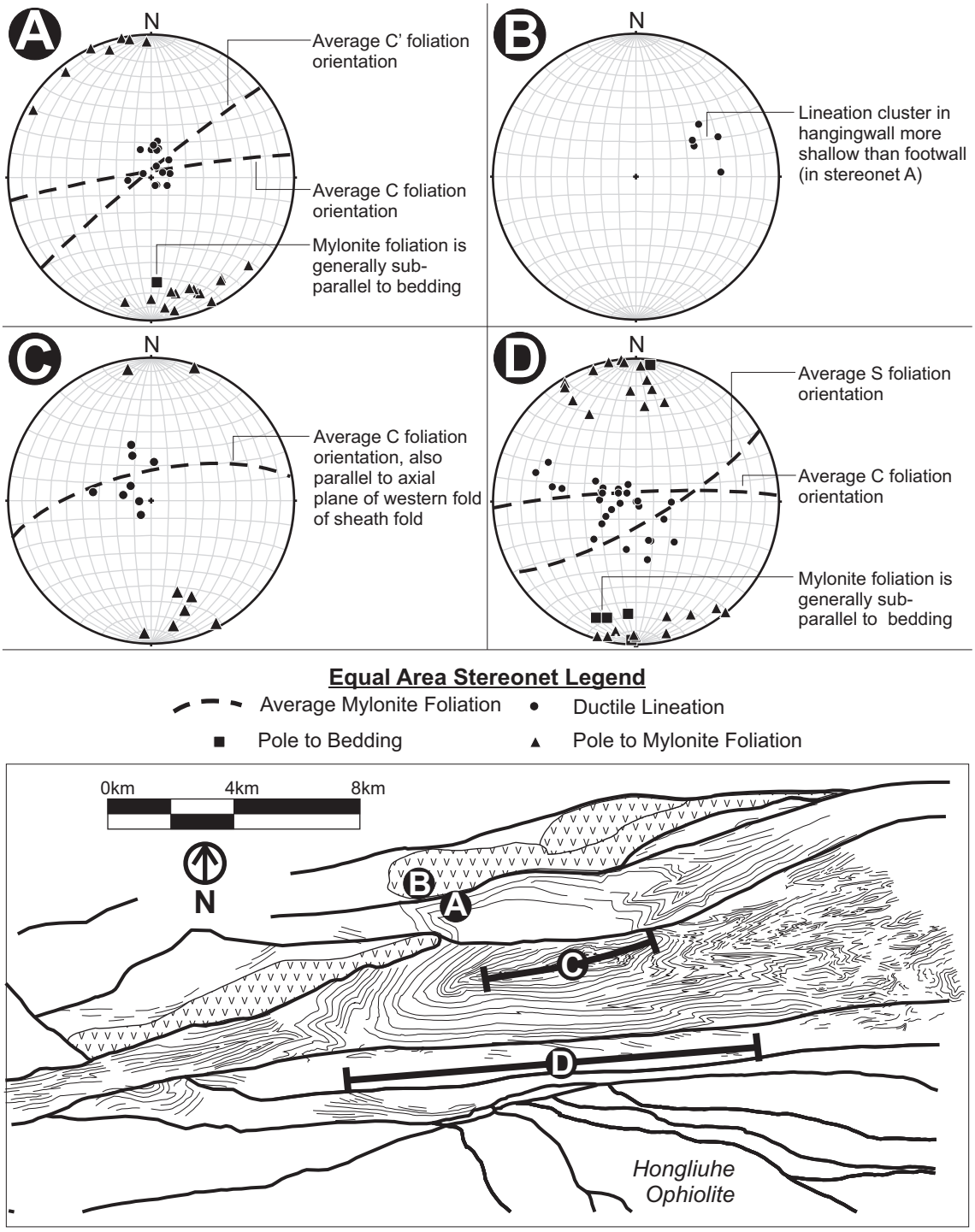

Figure 19: Stereonet plots of ductile faulting data: A) Mylonite data from the footwall of the Northern Internal Fault, located at 'A' on the inset map. The data shows a dominantly dip-slip orientation of movement along the fault. B) Stretching lineation data in the volcanic rocks that are the hanging wall of the Northern Internal Fault. The data shows a small strike-slip component in addition to the dip-slip shown in the footwall data. C) Stretching lineation and foliation data along the lengthwise axis of the sheath fold, located along the line marked 'C' on the inset map. D) Mylonite data for the Southern Boundary Fault Zone, located along the line marked 'D' on the inset map. The data shows a transpressive signature.

moderately towards east-northeast, were measured from the long axis of ellipsoidal lenses of volcanic material approximately one hundred meters north of the center of the shear zone. The rock does not hold a foliation, as disclosed in previous sections, making these lineations difficult to gauge. Only in one location were they exposed in three dimensions (Fig. 16C), in a weathered hollow of an outcrop (Fig.14B). Considering these lineations as relevant to motion across the fault, an added component of sinistral strike-slip motion would accompany the north-over-south movement inferred from deformation of the footwall.

3.1.2 The Median and Southern Internal Fault Zones

The Median and Southern Internal Fault Zones have the distinct similarity in that their outcrop is weathered to the point that it provides little structural information. Unlike the Northern Internal Fault, they involve blocks of sedimentary rocks in both the footwall and hangingwall. Topography around the Median Internal Fault plateaus north of the hilly eye-fold has provided a basin for modern lakes and stream to accumulate, thus weathering the fault zone. The outcrops that are exposed surrounding the fault zone do not show nearly as intense deformation as with the Northern Internal Fault. Only one sample of a pebbly conglomerate was recovered that shows a weak $C - C'$ fabric. The Southern Internal Fault Zone is completely weathered away, as it lies in the large river basin of the Hongliuhe. It is only noticeable in extremely weathered and friable outcrops of strongly cleaved and altered siltstones. Bedding traces are also visibly truncated against it on satellite imagery (Fig. 5). A significant structure providing evidence that they existed as brittle/ductile faults is the large-scale eye-fold in the center of the map area.

The central E-W axis of the large-scale eye-fold sandwiched between the Median Internal and Southern Internal Fault systems exhibits small bouts of ductile deformation. Stretching strain is observed, within one hundred meters or so of the axis in all lithologies, as stretched quartz grains in sandstones, slightly stretched pebbles in conglomerates and the general alignment of occasional clasts in finer lithologies (Fig. 17D). There is a sporadic cleavage parallel to the axial surface of the western synform of the eye-fold. Inconsistent with this, the easterly synform, with its hinge zone proximal to the fault to its north, has diverse cleavage orientations, most not parallel to the axial surface. In the eye-fold, the cleavage is expressed in sandstone and conglomerate lithologies that are close to the central axis. The siltstone stata that make up one of the inner elliptical bedding exposures of the eye-fold also bear the cleavage (Fig. 4).

3.1.2.1 *Structural Data and Kinematics of the MIF and SIF*

The faults bounding the eye-fold to its north and south, the Median Internal and Southern Internal faults yielded little structural data to this study. A single sample of a deformed conglomerate along the Median Internal Fault, just north of the hinge zone of the eastern fold of the eye, holds a moderately north-dipping foliation with a slight, down-dip stretching lineation. It holds a $C - C'$ fabric that indicates north-over-south motion across the fault. The Southern Internal Fault yielded no data to this study, and no structural samples, as there were no outcropping exposures found; reliable interpretation about its kinematics is not attempted in this study.

The data presented in Figure 19C represents proto-mylonitic foliations and their associated stretching lineations found within a zone straddling the E-W axial trace of the eye-fold. The lineations are relatively consistent, plunging very steeply to the NW, similar in orientation to the data from the fault to the north. This similarity supports the hypothesis that the eye-fold was formed as a response to north-over-south faulting of the blocks directly to the north. The amount of displacement across the fault is difficult to gauge but the creation of a ductile stretching response along the length-wise axis of the fold implies that the axial surface was beginning to yield and 'smear' as a precursor to proper fault development.

3.1.3 The Southern Boundary Fault Zone

The fault zone system bordering the Hongliuhe Ophiolite package in the South of the mapped area lies within the Hongliuhe river basin (of modern times) and has been weathered considerably, providing little fruitful evidence of its existence. On the geologic map (Fig. 4) it is represented by two close faults bounding the siltstone unit north of the ophiolite. The zone between the southern mapped fault trace and the Southern Internal Fault is interpreted to be the area under which a network of faults developed to accommodate strain – the traces are the best estimates of the dominant orientations of this wide shear zone. Again, weathering and fluvial sediment accumulation prevents good exposure of the faults. Figure 17E shows the existence of mylonite foliations with mantled porphyroclasts, though effective oriented samples could not be extracted due to the effects of weathering. From all observed locations of deformed sandstones and conglomerates in this area, no kinematics or evidence of deformation styles or mechanisms were observed or sampled. The mylonite foliation is sub-vertical with a steeply pitching lineation that was observed as slightly stretched conglomerate pebbles and quartz grains in sandstones (Fig. 17F). Various locations of deformed rocks were observed within a wide zone, at least 100 m, that trends ENE across almost half the breadth of the

map area, centered south of the eye-fold. The areas to the west and east were progressively more weathered from the effects of Hongliuhe river (which runs dry in the summer). It is a common feature to observe sub-crop of preserved decimeter-scale thick quartz veins throughout the length of the presumed shear zone, exposed by the weathering of the host rock.

3.1.3.1 *Structural Data and Kinematics of the SBF*

To generally describe the significant aspects of the fault zone data for the Southern Boundary Fault, referring to Figure 19D, there is a major trend towards E-W striking mylonite foliations with very steep northward dip directions. This fault zone, butting against the ophiolite package to the south, is generally wider with inconsistent, sporadic exposures of mylonitic rocks. The average trend of the shear zone orientation is sub-parallel to bedding, locally. The foliation may be gently folded, accounting for its slight spread. The surface traces of bedding on the satellite map (Fig. 5 and 19 *inset diagram, at bar marked 'D'*) show a slight large-scale waviness. Lineations, which mostly plunge sub-vertically, also show a slight spread towards shallower plunges. The lineations, departing somewhat from the average E-W mylonite foliation (that matches the fault surface trace trend), are spread along a second average foliation depicted in both Figure 19D and labelled 'Average S foliation'. This second averaged plane of the foliation shows the data that departs from the bedding parallel E-W trending shear zone's surface trace. It trends roughly thirty degrees from the average shear zone foliation. This trend would mark the secondary average foliation as an 'S' surface of a large scale S-C fabric. Samples from the Southern Boundary Fault yielded no kinematic data. An assumption of north-over-south dip-slip movement, if similar to the northern fault, would provide an opposite, dextral, strike-slip sense of motion when considering the less steeply plunging west-northwest lineations.

3.2 Folding in the Hongliuhe Group

Folding in the Lower Hongliuhe Group is a phenomenon closely associated with faulting. Folding is spatially linked to faulting, occurring either between closely spaced fault systems or proximal to larger fault systems. Some structures, such as the eye-fold, showing its nested elliptical bedding traces (Fig. 5B), imply temporal relations between folding and faulting as well. This large-scale eye-fold lies between two fault zones, the Median Internal Fault and the Southern Internal Fault, of which the Median Internal Fault is observed to have experienced brittle-ductile deformation within a narrow shear zone. To the north of the well-displayed eye-fold, just north of the Median Internal Fault, is another similar scaled shape of bedding traces that imply a second eye-fold, with more pronouncedly angular hinge zones. The strong

weathering of the outcrop within this structure was not conducive to measurement and analysis. In the interpretive cross-section across this area (Fig. 7), this is the antithetic anticlinal fold to the syncline of the eye-fold mentioned throughout this thesis. The next most significant zone of folding is an area proximal to the Southern Boundary Fault Zone that borders the ophiolite package, within the Permian rocks. This exposure is within a river bed, and outcrop preservation is poor to non-existent, though some measurements were taken.

3.2.1 Structural Data and Fold Morphology

The eye-fold approached in this thesis, the large well-traced fold visible in the satellite map (Fig. 5), is approximately 16 km in E-W breadth from hinge-to-hinge of the outermost traceable beds, and approximately 4 km in N-S width. It is synformal with steeply plunging axes for both the western and eastern folds which connect to make the eye shape. The western fold is visibly well defined with evenly spaced bedding sequences, whereas the eastern fold contains many chaotic, smaller-scale parasitic folds that are progressively poorly expressed further east as weathering disrupts bedding traces. The eastern strata of the fold, where proximal to the Median Internal Fault directly to their north, are deformed to be subparallel to the fault. This is a stark contrast from the bedding traces of the western fold, which are truncated against the fault to the north.

The western fold of the eye is a roughly cylindrical fold (Fig. 20A) with a consistent axial planar cleavage. The axial plane trends WSW and dips steeply north. The fold axis plunges steeply to the NE, consistent with measured bedding/cleavage intersection lineations. The eastern fold of the eye is a near cylindrical fold, with a slight conical aspect. The bedding is mostly sub-vertically dipping, and the poles-to-bedding plotted on a stereonet (Fig. 20B) spread around the primitive slightly more than is possible with a cylindrical fold. The hinge of the fold is sub-vertical, with parallel measured bedding/cleavage intersection and outcrop-scale fold hinge data. The axial plane trends NE and dips vertically. Cleavage measurements, the poles of which are plotted in the same figure, are spread along the same profile plane as the bedding poles.

Throughout the Hongliuhe Group, fold orientations are relatively consistent with the East and West eye-fold orientations. Figure 20C and E show structural data of folds observed in different locations, south of the eye-fold and separated from it by two faults. These folds, with orientations of features similar to those of the western limbs of the eye-fold, are smaller outcrop scale folds. Figure 20D shows structural data of a fold observed to the south and east of the

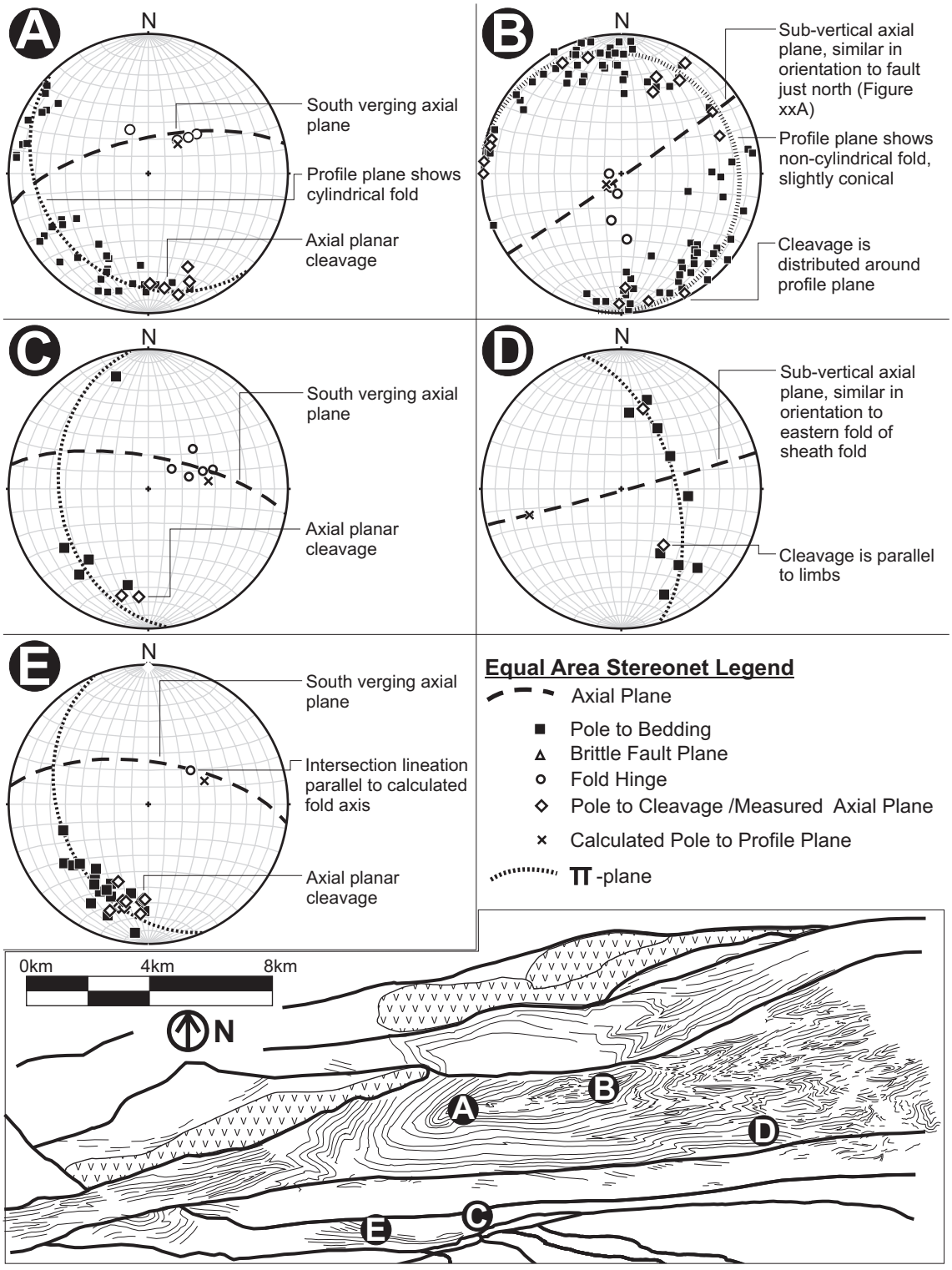

Figure 20: Stereonet plots of folding in the Hongliuhe Group: A) Western side of the sheath fold B) Eastern side of the sheath fold C) Cylindrical fold of similar orientation to the fold in A, located near the southern fault zone. D) Cylindrical fold of similar orientation to the fold in B, located near the southern fault zone. E) Cylindrical fold located near the southern fault zone, with an orientation similar to A but with a spread of lineation data that may indicate another subsequent overprinting fold.

main sections of the eastern eye-fold limbs, yet within the same fault-bound block. It depicts a cylindrical fold with a similarly oriented axial plane to the eastern fold of the eye, though the (calculated) fold axis is not sub-vertical, rather plunging moderately towards WSW. This may give clues as to the development of the orientation of the eastern half of the eye-fold during its protracted exposure to fault displacement along the Median Internal Fault.

3.2.2 Nested eye-fold Ellipticity Variance

Using satellite images (Fig. 5) nested bedding traces of the eye-fold were outlined at various distances from the center to provide a gauge of the variance of their ellipticity (Fig. 21). The measured lengths of the primary axes of three of the concentric eliptical bedding traces

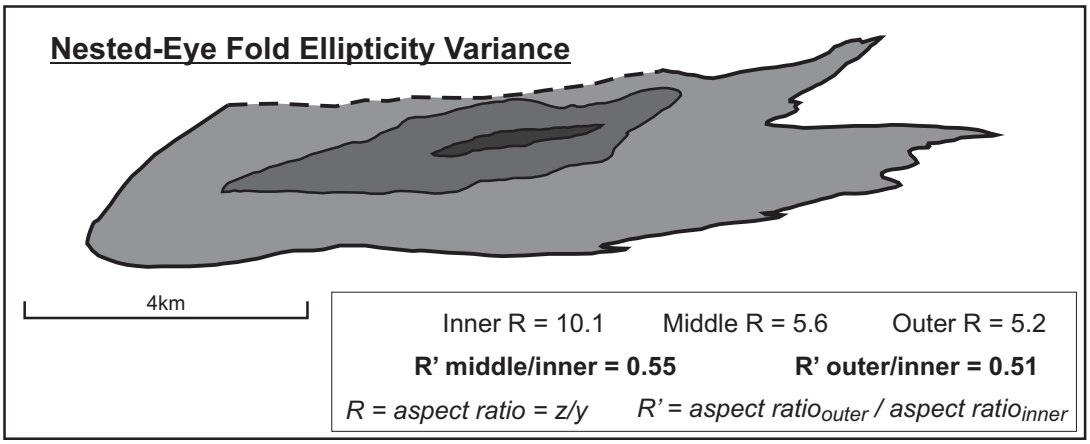

Figure 21: Variance in ellipticity from central nested eye-fold to outer rings. The higher aspect ratios of the outer layers, compared to the inner layers, shows its kinship to ductile sheath folds associated with shear zones. The dashed line indicates the trace of the Median Internal Fault.

were compared in ratios (R). The aspect ratios of the three ellipses, from the innermost to the outermost are $R_{inner} = 10.1$, $R_{middle} = 5.6$ and $R_{outer} = 5.2$. It is conclusive that the ellipticity decreases outward from the center. The ratio of aspect ratios from inner to outer traces gives a measure to this variance and has been given the definition $R' = \frac{aspect\ ratio_{outer}}{aspect\ ratio_{inner}}$ (Alsop and Holdsworth, 2006; Alsop et al., 2007). The comparison of the ellipticity between the middle trace of Figure 21 and the inner trace is $R' = 0.55$, showing that the inner is significantly more elliptical. The comparison of the ellipticity between the outer trace and inner trace is $R' = 0.51$, showing a similar ratio, yet even more extreme. It must be noted that the outer trace is not a complete bedding trace, as the fault on its north side truncates the bedding in the west. The cusp in the upper left corner of the trace in the diagram (Fig. 21) is the point

where they join. If the bedding traces had been complete, the ellipticity of outer ring would have been less, and the variance more.

3.3 The Xingxingxia Road-cut Cross-Section

This section continues with description of deformation in the upper sections of the Hongliuhe Group with an example of an isolated outcrop found along a road-cut near the small truck-stop town of Xingxingxia. The Hongliuhe Group at this point is approximately 50 km along strike to the northeast of the mapped area previously analyzed. The freeway that runs from the town of Liuyuan to the town of Xingxingxia cross-cuts the Hongliuhe Group sub-perpendicular to its strike. The Hongliuhe Group does not outcrop extensively along this freeway and outcrop quality is typically poor when it does, so no attempt to map the general area was made. No significant large-scale structures are visible in satellite imagery. A complete sectional traverse along the freeway of the entire Hongliuhe Group exposure was conducted by observing the outcrops along the freeway and examining the types of lithologies and associated structure. The one small outcrop reported in this section was unique in the quality of structure exposed along its face, exposed from the excavation to cut a path for the freeway through the rock. Of all outcrops along the freeway that were observed, it is the only one of significance to this study, and the only one reported. The lithologies pertaining to this outcrop consist of sandstones, siltstones and silty-mudstones; conglomerates are distinctly absent. This is characteristic of the Luweijing Formation of the Hongliuhe Group classification scheme by Li et al. (2006). The intact part of the exposure, which measures approximately 200 m in length, shows structural features on both sides of the freeway, though only 136.5 m of the western side of the road was mapped at a scale of 1:50 to accurately show the lithology and structural features consistent with fold-and-thrust belt style deformation contained within this unit.

3.3.1 Fold-and-Thrust Belt Style Deformation in the Hongliuhe Group

Strata in this cross-section Hongliuhe Group generally dip moderately northward, on average. Their average dip is shallower than the strata previously discussed, in the map area near Hongliuhe. The deformation observed in this section is consistent with its higher stratigraphic position in the upper sections of the Hongliuhe Group (possibly Luweijing Formation). It contains isolated zones of ductile deformation (shear folding), no evidence of crystal-plastic deformation at the grain scale, and considerably more low-angle faulting than in the Hongliuhe map area. The road-cut outcrop observed and mapped depicts a fold-and-thrust belt style of deformation, suggesting that the structures observable now appear to have been a brittle-ductile response to a N-S compressive stress that accommodated shortening and thickening of the unit through a series of thrust faults and concurrent footwall folds, imbricate thrust fans and duplexes (Fig. 22). Though mapped at a scale of 1:50, this section is displayed at a scale of 1:100 due to the reasonable limits of paper publication.

The three lithologies involved in this cross-section are a clean brown-grey arenitic sandstone, a grey sandy-siltstone, and a dark purple-grey silty-mudstone. Contacts between the lithologies are sharp and primary bedding features such as regular laminations in the siltstone still exist. Such laminations occur as very thin bands, millimeters thick, of brown silt alternating with the grey siltstone beds, each up to 2 or 3 cm thick. Sandstone beds are generally 10 cm to 1 or 2 m thick, segregated by sets of siltstone beds from centimeters thick up to 1 m thick. The silty mudstone is present in the least amount, comparatively, and exists in sporadic beds up to approximately 1 m thick. The maximum grade of metamorphism that has affected these lithologies is very low greenschist facies as a slight sheen of muscovite or illite minerals can be observed on some surfaces, and constitutes only a very small percentage of the volume of the rock. Small veins of quartz and carbonate are spread throughout the outcrop, but are not widespread or dense in any area. They are more common near fault zones.

The paved road for which this section was cut bears NNW–SSE, or 334–154 degrees. As the profile planes of the folds depicted dip steeply to sub-vertically and strike in the 130 to 165 degree range, the mapped or photographed structural features are very close to representing their true profiles.

3.3.2 Xingxingxia Cross-section and Structural Domains

The structural cross-section has been divided into seven domains, as labeled in Figure 22, to best isolate packages originating at different stratigraphic levels, now bounded by faults, and to provide a basis for analytical description. The domain brackets in Figure 22 are positioned above the outcrop, but the limits of the domain are considered the faults, marked in yellow, whose traces, at the top of the outcrop, align with the ticks of the bracket.

It is the author's observation and judgement that, though the amount of fault displacement is not directly apparent over most of the faults present, the individual sections of each domain are not completely exotic with respect to each other. The system as a whole represents a relatively homogeneous strain response (at the formation scale) from an originally cohesive or

---

Figure 22 *(following page)*: The Xingxingxia road-cut cross-section. The 136.5 m structural section has been divided into seven fault-bound domains as labeled. The cross section has been mapped without any vertical exaggeration. The dashed boxes labelled with letters show the respective frames of photos in Figures 24, 25 and 26.

Xingxingxia Road-Cut Structural Cross Section

Location: Gansu Province, People's Republic of China
Road Bears 154° →
Scale 1:100

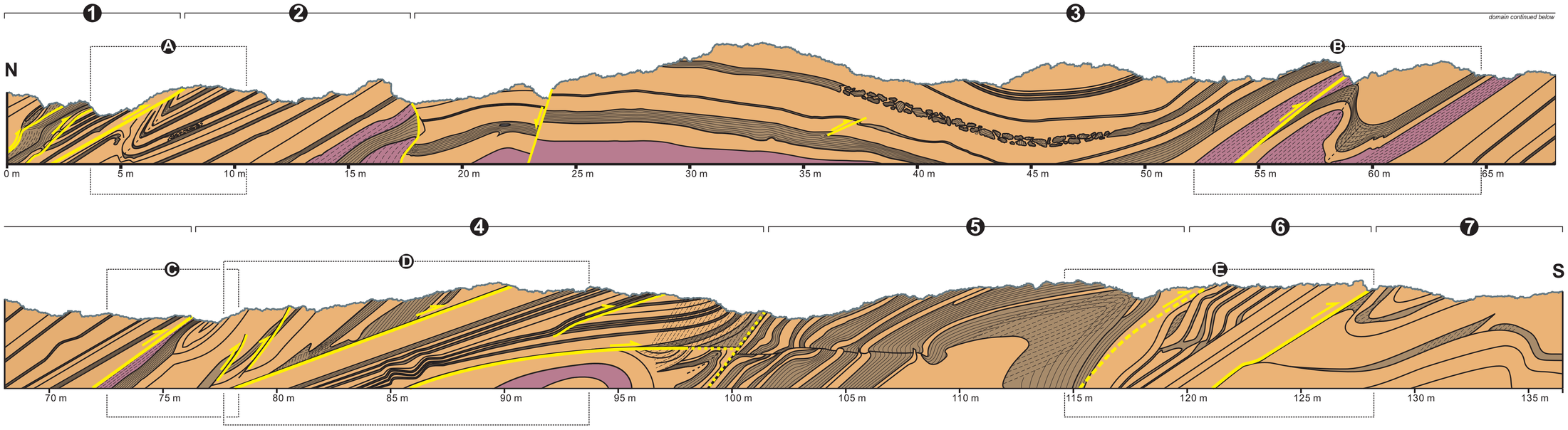

Legend

Lithology

- Silty Mudstone
- Laminated Sandy Siltstone
- Sandstone

Symbology

- Cleavage
- Thrust Fault with movement direction *Observed / Inferred*
- 1 Structural Domain Markers (refers to text)

continuous section of the Hongliuhe Group.

3.3.2.1 *Domain One*

The main structural feature of domain one consists of a series of fault zones within the siltstone material that shows imbrication, or a steepening of the fault system towards the north side. It appears that the main effect of this is to accommodate shortening through thickening of the siltstone package. Fault displacement is evident through the effects on the more competent sandstone unit, as it is boudinaged close to the middle fault. The sandstone boudins show the effects of necking with deflections of the siltstone foliation into and between the necks. Bedding, fault and cleavage measurements plotted on a stereonet show the overall steepening of the bedding and faults due to the imbrication and a cleavage parallel to the axial plane of folds in subsequent domains (Fig. 23A). The southern limit of domain one is a low angled thrust fault that overrides domain two, serving as the floor thrust upon which the imbrication sequence breaks and steepens.

3.3.2.2 *Domain Two*

Domain two consists of a section of moderately north-dipping strata, a sequence of sandstone and siltstone beds that typifies the structural attitude of the area. The top of the domain, the northern end, borders the thrust fault at the south end of domain one and exhibits a tight fold (Fig. 24A). There is a thickening of siltstone beds in the hinge zones. The hinges transition from rounded to angular closer to the fault. The increasing angularity of the fold closures closer to the fault is interpreted to be a product of drag induced deformation in the footwall from north-over-south displacement of the hangingwall along the fault. The axial surface curves towards parallelism with the fault plane higher in the outcrop, where it is closer to the fault, but generally coincides with the orientations of subsequent folds in latter domains. It verges at a moderate dip towards the southwest (Fig. 23B), but is not parallel to the fault; the fault is parallel to the southern limb of the fold. The north limb of the fold in the footwall of the northern boundary fault, at the upper reaches of the outcrop, is truncated against the fault: a footwall cutoff. At the base of the outcrop the footwall strata are acting as a footwall ramp. A fold closure is partially obscured by rubble in the footwall, but they can be seen to approach the pattern for this fold in the footwall to be a 'Z' shaped fold. This transition from a footwall ramp to cutoff along the fault implies that an existing fold must have been truncated: a mature break-thrust fold (Thorbjornsen and Dunne, 1997).

The base of the section shows the introduction of the purple-grey silty-mudstone, the least

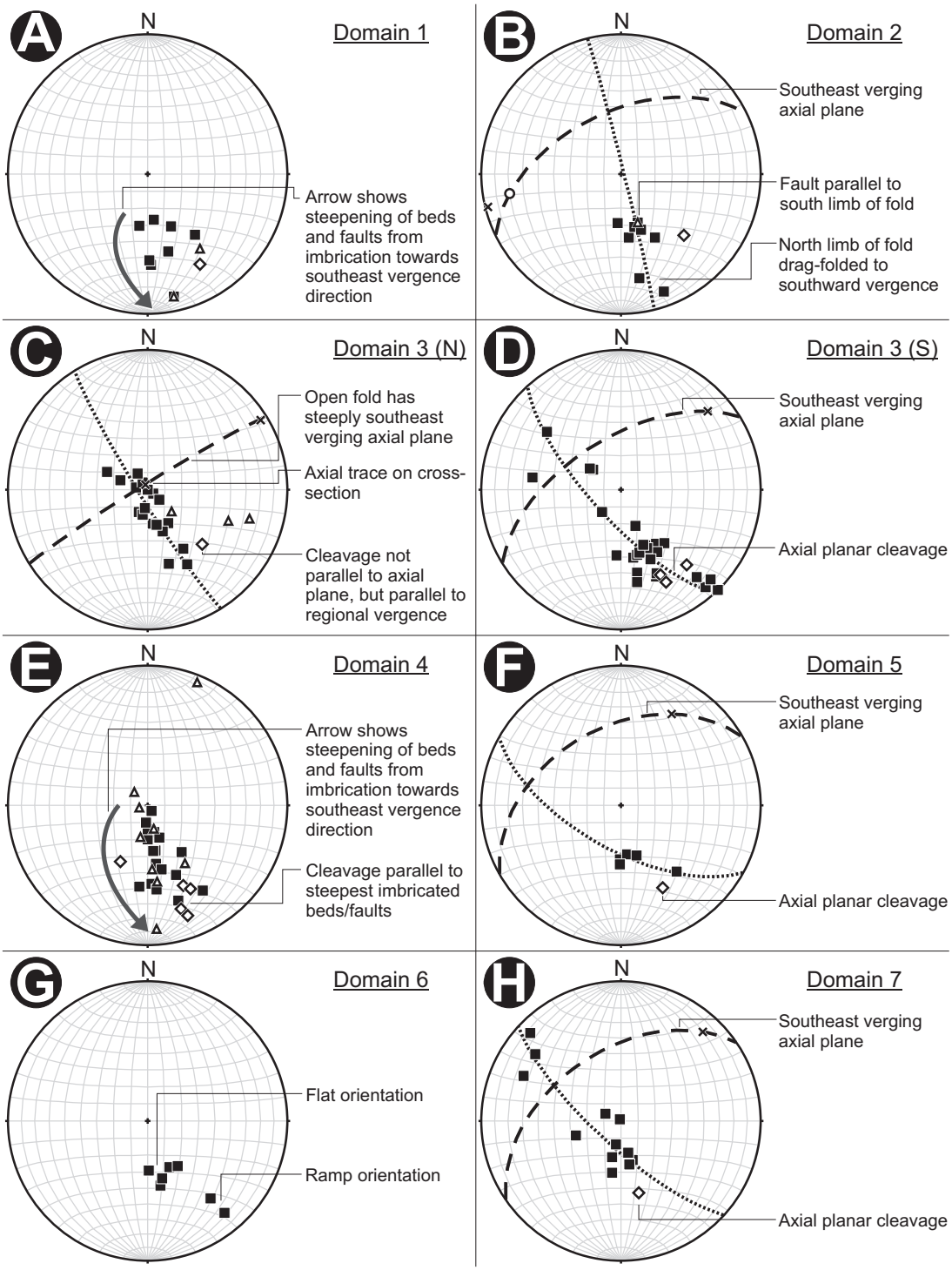

Figure 23: Stereonet plots of structure in the Xingxingxia cross-section: A) Imbrication in Domain 1 B) Folding in Domain 2 C) Open fold in Domain 3 D) Shear fold in Domain 3 E) Imbrication in Domain 4 F) Fold in Domain 5 G) Duplexing in Domain 6 H) Folding in Domain 7. *Legend from Fig. 20 applies to this figure.*

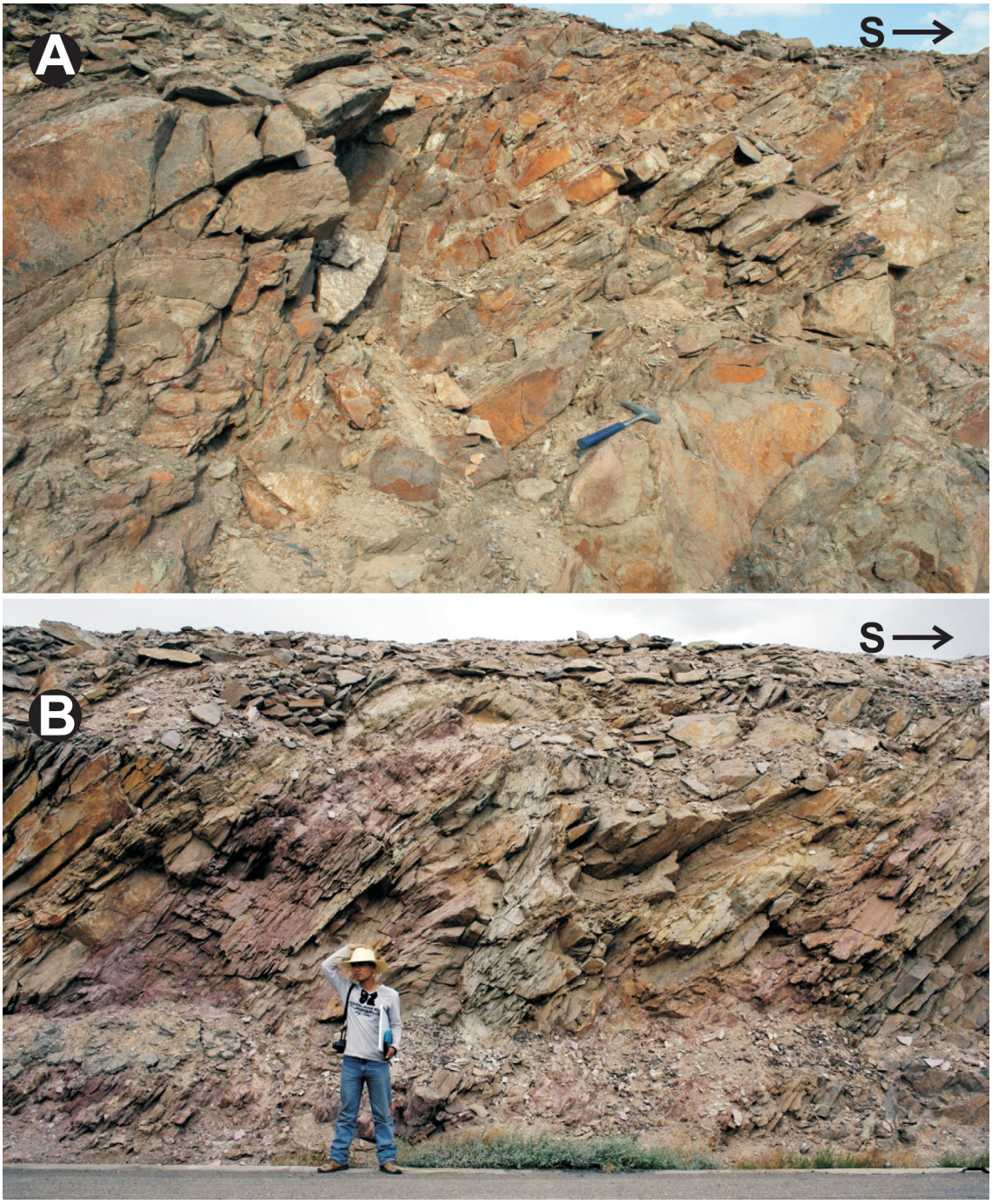

Figure 24: Images of structures along the Xingxingxia road-cut: A) Angular shear fold in Domain 1 B) Rounded similar fold in Domain 3

competent unit, that hosts a strong cleavage and the domain's southern bounding fault zone. The fault plane that bounds domain two on the southern end truncates a section with a mudstone to siltstone to mudstone sequence that is not seen elsewhere in the outcrop. This leads to the conclusion that there has been enough displacement, of unknown direction, across this fault to allow such juxtaposition of two different stratigraphic sequences from domains two and three.

3.3.2.3 *Domain Three*

The length of domain three, considerably longer than all other domains, shows a broad, flat-lying, gently and openly folded section that continues with the south limb faulted and ramped over a repetition of its strata towards the southern end of the domain. The strata at the south end of this domain are in the regional orientation of the formation in this area, dipping moderately to the north. The one thrust fault not bounding this domain, at the 55 m mark, is a ramp that initiated from the stratigraphic level of the mudstone layer and propagated up-section. In the footwall there is a very well developed and displayed 'Z' shaped similar or shear fold. A photograph showing the well-structured morphology is seen in Figure 24B. The morphology of the fold shows an increase in thickness at the hinges in the less competent units, namely the siltstone, and a decrease in thickness in the central limb at the inflection of the 'Z' shape. The siltstone contains a well-developed axial planar cleavage. The siltstone strata in the north limb of the fold are visibly truncated against the fault, a relic of its original footwall cutoff orientation. This implies that the fold was formed as a response to strain from fault displacement, and did not exist as an intra-foliar fold prior to faulting. This interpretation is supported by the observation that the axial planes of the fold are more or less parallel to the thrust fault (Fig. 23D). The structural data for the open fold has a steeper south-verging axial plane with a similar trend to other axial planes and faults in this section (Fig. 23C).

3.3.2.4 *Domain Four*

There exists similarities in lithological sequences in domain four to the previously described northern domains but complicated imbrication disrupts the stratigraphic continuity and begs classification as its own domain. The northern bounding fault of this domain is hosted in mudstone and siltstone and has produced an isoclinal fold in sandstone in the footwall (Fig. 25C). South of this structure is a series of structures showing thrust imbrication. The rock underlying the nearly flat-lying basal ramp fault appears to be a series of folds, the first a broad, rounded fold of a sandstone and mudstone sequence that is reminiscent of sections in domain three. The limited exposure disallows correlation between the stratigraphy. It cryptically folds

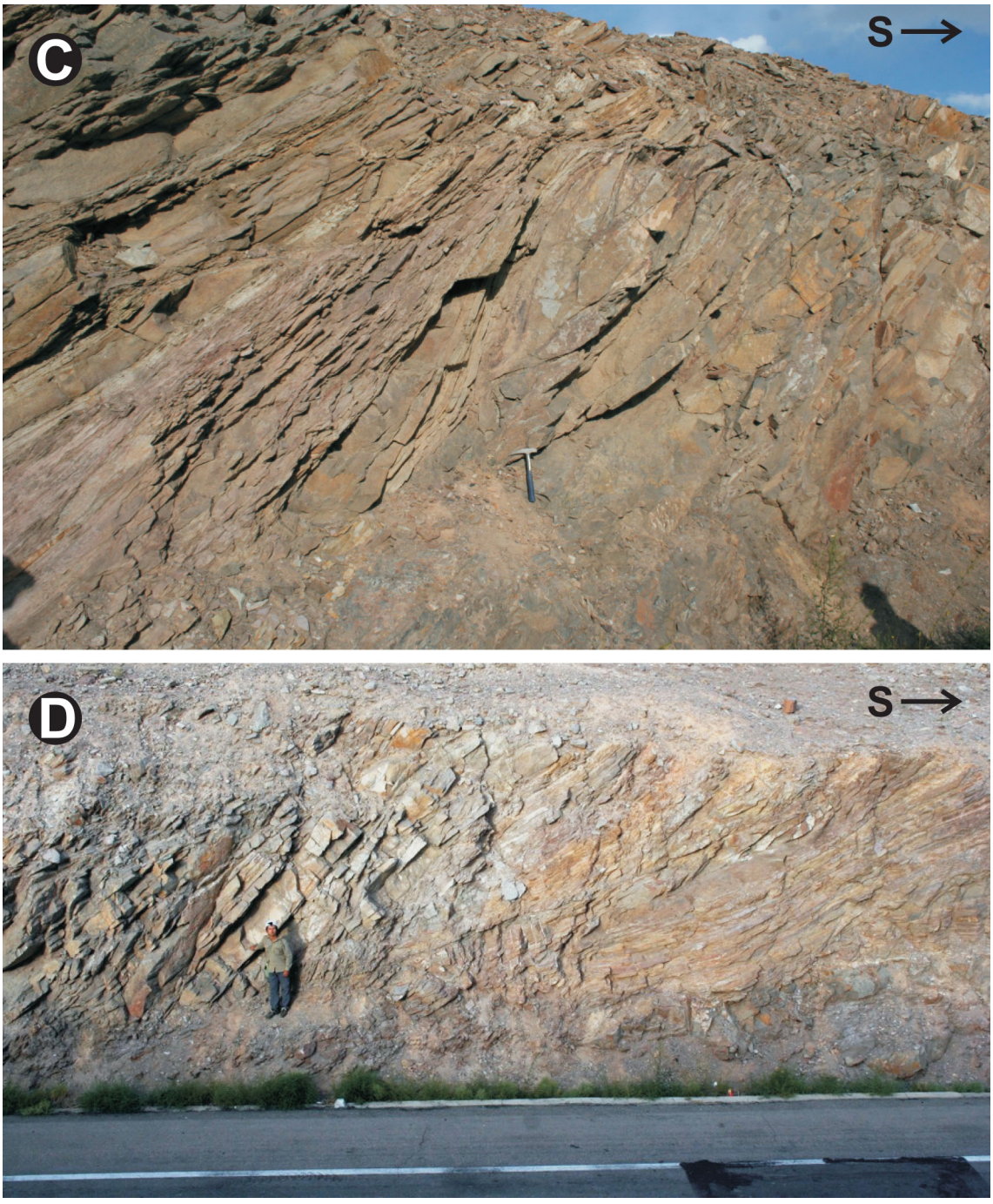

Figure 25: Images of structures along the Xingxingxia road-cut: C) Isoclinal fold in sandstone in Domain 4 D) Imbricate thrust fan in Domain 4

downward and truncates the base of a second fold that is pressed up against the beginning of the strata of domain five to the south. Rubble obscures the contact between these two folds, so their relationship and contact remains mysterious. The fault system that is contained in the strata that overlie this ramp show a progressive steepening of the faults northward (Fig. 23E) and show both footwall cutoffs and hangingwall cutoffs at the faults (Fig. 25D). Bedding is progressively steepened northward as well, matching either of the bounding faults for each set of strata. Fault displacements appears to be more than each fault surface length visible in the outcrop, with the exception of the two northern-most, small sub-vertically dipping faults with small, visible offsets. Cleavage, focused in rock towards the southern end of this domain, is sub-parallel to the axial planes of most other significant faults in other domains, and also to the steepest of the imbricated beds and faults in this domain. The boundary of domain four in the south is an inferred fault which is interpreted to be a steep ramp with northern strata being faulted over the south. This would not be an ideal angle for thrusting, which implies that it may not be a large displacement fault which in turn may have induced the response to its lack of strain accommodation as thrust imbrication within domain four.

3.3.2.5 *Domain Five*

There is a significant change in lithology from domain four to domain five into a section with siltstone as the dominant lithology. Interbeds of sandstone are thin and relatively evenly spaced. From the northern boundary towards the south dips of beddings shallow until near parallelism with the northern limb of the large close fold displayed in the siltstone. The fold shows a thickening at the hinge and appears rootless on its northern limb. There is a strong axial planar cleavage hosted in the siltstone that is not evident in the sandstone. This fold is unique in the outcrop, as it does not appear to be associated as a folding response in the footwall of a fault. The outcrop directly to its north is rubbly and heavily fractured, and may be a more distributed fault system, or even outer strata of the fold, which would mean it is a footwall fold of the fault separating domain five and six. Alternatively it could be considered to be a folding response in the hanging wall of the fault that is the southern boundary of the domain, inferred to be just to its south. This end of the domain is also heavily fractured and is considered to be, in conjunction with the heavily cleaved southern limb of the fold, the fault system along which displacement occurred to impart the structures visible in the next domain. An observation to support this is the trace of the thin sandstone bed between the siltstone beds involved in the fold: it is noticeable that the bed is necked and terminally boudinaged in the southern limb, indicating that the south limb has undergone extension. This can be seen in the upper left corner of Figure 26E.

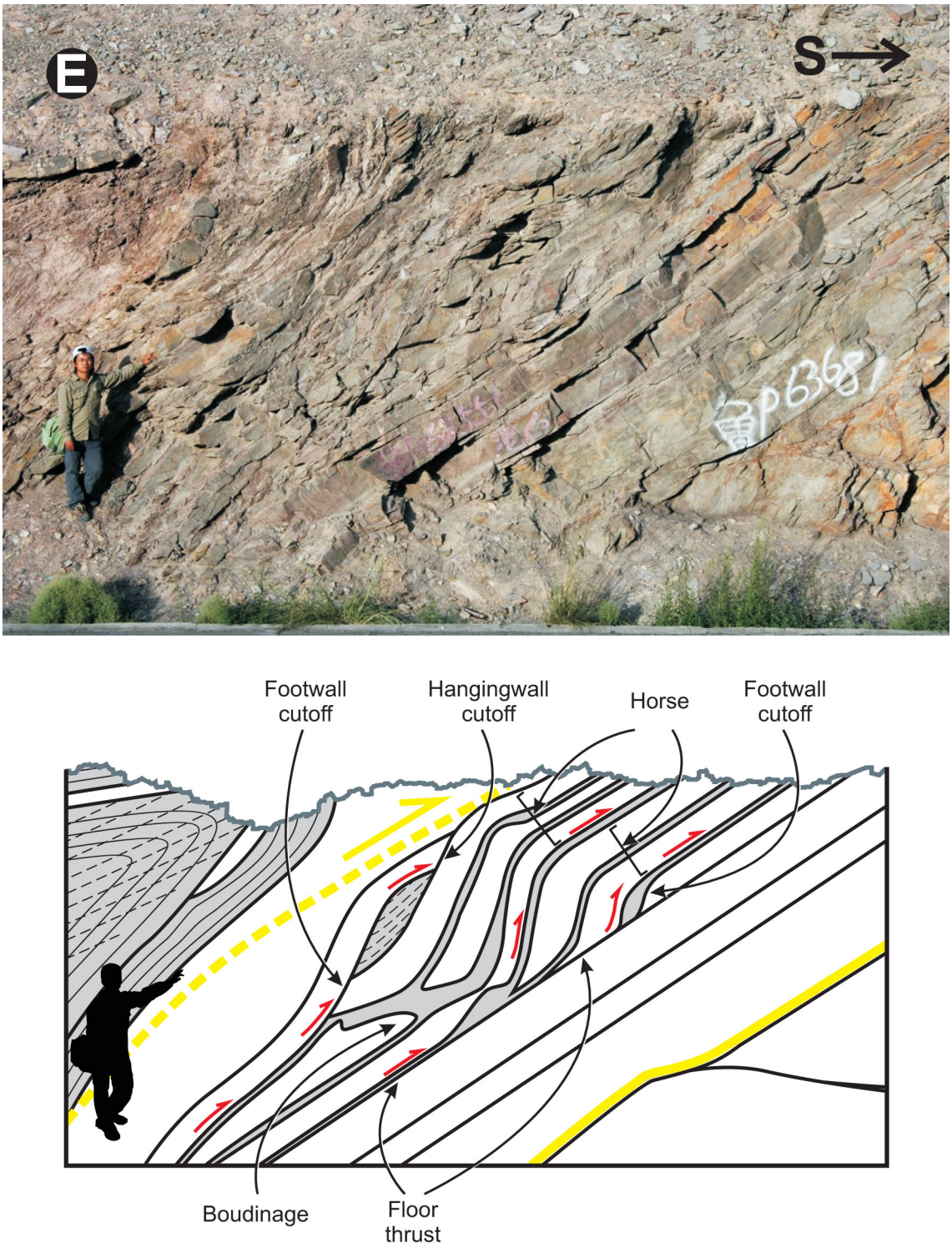

Figure 26: Images of structures along the Xingxingxia road-cut: E) Duplexing in Domain 6. Inset diagram shows schematic of faulting system with the duplex structure.

3.3.2.6 *Domain Six*

The duplexing visible in domain six is some of the most unique evidence of this section exhibiting fold-and-thrust belt style deformation. A photo of the domain and this structure can be seen in Figure 26E, with an accompanying diagrammatic interpretation of the fault system. The structure mapped shows a set of horses, some layers with boudinaging, and an incompletely formed horse bordering the roof thrust at the top (see Figure 26 diagram). Horses are found in small sections of interbedded sandstone and siltstone, and (apparently) not all siltstone layers have acted as slip zones. The effect of duplexing in this section directly accommodates up-dip shortening and dip-normal thickening. Flats in this structure are generally bedding parallel (with respect to both strata down-section in this domain, and the regional bedding trend) and ramp dip more steeply, a little more steep than cleavage trends in this cross-section, and trending a little more westerly, giving them a unique orientation (Fig. 23G). The southern boundary of this domain is meters down-section of the basal ramp and is a thrust fault.

3.3.2.7 *Domain Seven*

The thrust fault that borders domains six and seven shows a large, asymmetric, tight fold response in the footwall (Fig. 23H). Though the northern limb is short and truncates against the fault ramp, and though in the south the next similarly oriented limb continues underground, the fold makes a larger scale 'S' shape. The axial surface trace on the outcrop wall is not linear and deflects through weaker lithologies, namely the siltstone. The siltstone also holds an axial planar cleavage.

3.3.3 Xingxingxia Cross-section Restoration

The main effects of deformation in the Xingxingxia cross-section is accommodation of horizontal shortening through rotation of beds and subsequent up-dip faulting which creates thickening, perpendicular to bedding, through imbrication, duplexing and folding. This must mean that restoration of portions of the section to pre-deformation orientations can provide a measure of the amount of shortening (Dahlstrom, 1969; Hossack, 1979; Wickham and Moeckel, 1997). The exposure of the section is very limited and only domain three was approached for restoration (Fig. 27). The other domains are considerably shorter and are bound by faults which separate sections of strata that may not have originally been laterally continuous. The short length of the other domains implies that a restored section would have a large amount of uncertainty or margin of error inherent from measurement and mapping limitations. Without

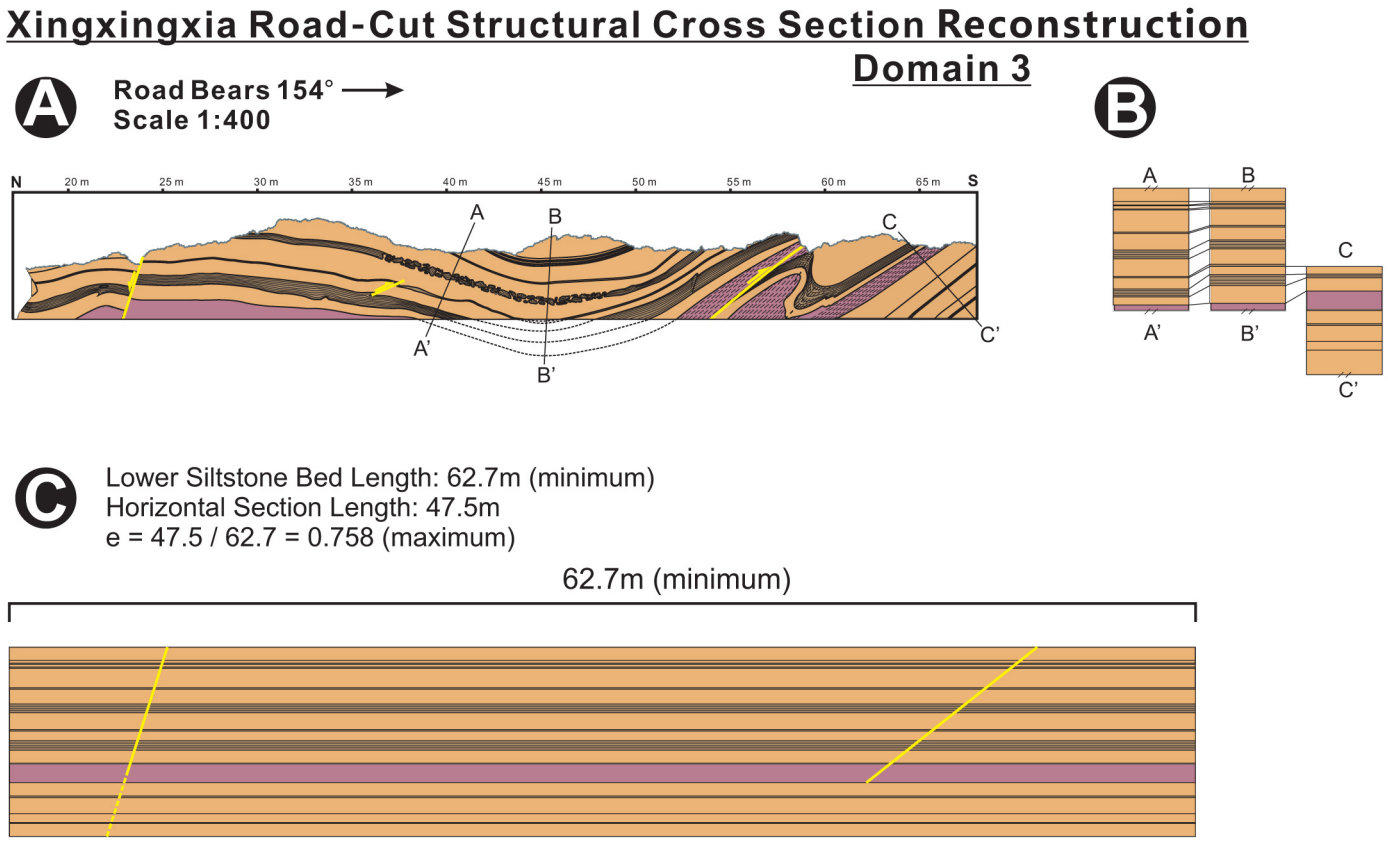

Figure 27: Restoration of Domain 3 of the Xingxingxia structural cross-section: A) Domain 3 with lines depicting the locations used for thickness estimations. B) Stratigraphic thicknesses based on the lines noted in A C) Restored section showing original length and original locations of faults in Domain 3

lateral continuity of the strata between the domains restored sections would not be able to be joined together in an attempt to reduce the uncertainty in restored short domains. Domain three, with its unique aspect that it is long and contains a fault and fold structure whose strata were evidently originally continuous provides a section with less inherent error. It is also not representative of the entire outcrop, and is unique in that it contains the lowest density of shortening-accommodating structures seen throughout the cross-section. If the remainder of the geologic formation has a similar distribution of structures the restored section of domain three gives us an absolute minimum estimate of the shortening in the region, and not an average or maximum.

The restoration attempt shown in Figure 27 was approached through finding an average bed thickness from key places in the domain and a measured length of the top contact of the central, thicker siltstone unit. The siltstone unit was chosen as it is continuous and traceable throughout the length of the domain. The bed thicknesses in the restored section, Figure 27 C, were calculated from averaging the thicknesses of beds at the inflection point and hinge zone of the large, broad, open fold (lines A to A' and B to B' in Figure 27 A and shown in mock sections in Figure 27B). These locations were chosen to account for thinning or thickening of different strata in the fold hinge or limbs, which appears to be minimal in this open fold. As the lower contact of the mudstone stratum is not visible north of the fault zone a section perpendicular to bedding was taken along the line C to C' in Figure 27 A to estimate the lower lithologies (with mock sections shown in Figure 27B). Figure 27 C shows the restored section with the positions of the faults along the line length that they currently are. Note that due to the unknown displacement along the fault, this length is a minimum estimate based only on the material visible in outcrop. The reconstructed section illustrates the aspect that the southern fault acted as a ramp for thrust faulting of all overlying strata and that the mudstone layer acted as the basal detachment. The measured length of upper contact of the siltstone bed is 62.7 m. The horizontal length of the section from endpoint to endpoint of the contact is 47.5 m. Calculated horizontal shortening strain is $e = -0.242$, as a minimum measure of shortening, considering the unknown fault displacement.

4 Discussion

The lifespan of deposition, lithification and deformation experienced by The Hongliuhe Group was brief with respect to the protracted sequence of geologic events that amalgamated the Central Asian Orogenic Belt. Its record marks the development of the final collisional processes in the Beishan. This study explores the relationships between deformation and the lithology at different stratigraphic levels in the Hongliuhe Group with the purpose of elucidating ideas about its tectonic setting and to quantify the effects of the final collision between the terranes of the Gongpoquan arc-accretionary system.

4.1 Hongliuhe Group Stratigraphic Classification Scheme

The conclusions proposed by the Hongliuhe Group stratigraphic classification scheme of Li et al. (2006) are sharply contradicted by this study. The work performed for this thesis is limited by its mapping bounds to the area north of the Hongliuhe mélange zone; the Hongliuhe Group extends along strike in each direction for another 50 km or so, therefore the study of Li et al. (2006) may be based on observations not made in this study. Portions of the stratigraphy proposed by this study (Fig. 6) match well with the characteristics of the formations of Li et al. (2006) but their order is redefined by structural interpretation.

A caveat of this stratigraphic reconstruction is that, due to the poor exposure of some strata (e.g. in the modern-day Hongliuhe River basin), it is unknown if there are repetitions of some lithologies. Figure 6 is a reconstruction based on the assumption that there is no repetition, as none were conclusively noticed. It is also probable that sections are missing from between the fault bound blocks.

The Hongliucun Formation is easily recognizable with its volcanic assemblages, yet this study places it at the base of the stratigraphy because of its role as the hangingwall of the Northern Internal Fault. This shear zone is the widest in the Hongliuhe Group and shows evidence of prolonged ductile deformation. It is reasonable to infer that, with north-over-south motion, faulting juxtaposed the older Hongliucun Formation against the conglomerates of the footwall. This NIF footwall section of conglomerates are similar to both the Hexi Formation and the base of the Luweijing Formation, which is where the existing classification scheme fails. This package of conglomerates bound between the Northern Internal Fault and the Median Internal Fault is proposed, by this study, to be a continuation of the small sliver of conglomerates unconformably overlying the Hongliucun package, at the very north of the mapped area (at the north end of the section line in Figure 4, at the north end of the section in Figure 7, and just

below the first fault break in the stratigraphic column, Figure 6). The distribution of lithotypes of the conglomerate clasts are similar between the two packages. As graphically depicted in the stratigraphic column (Fig. 6) it is unknown if sections are missing due to faulting. This stratigraphic organization fits with other studies: the work of Pan et al. (2008) provides Late Carboniferous–Early Permian dates of the volcanic rocks at the base, and the studies of Li et al. (2006) give paleontological evidence from the Hexi Formation that the Hongliuhe Group is Early Permian in age. The fault-compensated stratigraphic organization of this study puts the slightly older volcanic rocks under the younger formation, instead of *vice-versa*.

The remaining section of the Hongliuhe Group between the Median Internal Fault and the Southern Boundary Fault (except a small portion noted in the next paragraph) correlates well with the Luweijing Formation of the Li et al. (2006) scheme. Therefore, the faulting of the Southern Internal Fault is not constrained, and may have been misinterpreted in the stratigraphic reconstruction (Fig. 6). The similarities to the Luwejing Formation are thoroughly consistent; the section bears thick sequences of rhythmically bedded sandstone and siltstone strata and considerable deposits of the monomictic granitoid conglomerate. The strata depicted in the Xingxingxia structural cross-section are most likely Luweijing Formation, as their lithological descriptions are consistent with the classification scheme of Li et al. (2006).

The Hongliujing Formation, the uppermost formation of the Li et al. (2006) classification, does not hold the same position in the stratigraphic column of this study (Fig. 6). Li et al. (2006) state that the Hongliujing Formation is contained within the center of a large synform, which is presumably the eye-fold of this study. The lithologies of the central units of the eye-fold are consistent with this formation designation; they consist of siltstones, some with calcareous matrix, and calcareous boulder conglomerates. This small section is noted on the stratigraphic reconstruction (Fig. 6).

4.2 Hongliuhe Group Tectonic Setting of Deposition

The reconstructed stratigraphic sequences of the Hongliuhe Group proposed by this study (Fig. 6) exhibit a gradual, general fining upwards sequence, with decreasing amounts of conglomeratic rocks and increasing amounts of sedimentary rocks that represent nearshore oceanic depositional environments. Its base is a polymictic conglomerate of metamorphic rock clast types that unconformably overlies a volcanic rock. Interpreting that this is a continuous section, which is not missing large amounts of strata due to faulting, its structural and sedimentological characteristics imply a foreland basin setting for deposition (Cross, 1986; Covey, 1986; DeCelles

and Giles, 1996). The concurrent folding and faulting consistent with a fold-and-thrust belt style outlined in the structure section support this interpretation, as do other sedimentological data. The change in lithotypes of the conglomerate clasts from polymictic metamorphic types to monomictic granitoid type (with small amounts of monomictic limestone in between) reflects a gradual unroofing of the terrane involved in the collision, also an expected foreland basin feature (Ver Straeten, 2010). The polymictic mix of types reflects the assortment of lithotypes that would have existed pre-orogeny, and the deeply emplaced younger plutons would not have been exposed as a sedimentary source until after a considerable amount of erosion had occurred. The change in clast types may reflect a change in the source of sediment, but considering the sub-angular nature of many of the clasts, and the large boulder size of some, sources were likely proximal. The possibilities for provenance should limited in scope to proximal terranes.

4.3 Hongliuhe Group Provenance

This study does not focus on elucidating the provenance of the Hongliuhe Group, but some of the lithological observations may provide some constraints on it. The basal conglomerate clasts, including mylonitic gneisses, strained tonalites, metamorphosed siltstones, schists, and marbles imply sediment input from one of the more mature sub-arcs in the Gongpoquan composite arc. The Hongliuhe Group lies within the bounds of the Mazongshan arc terrane, as designated by Xiao et al. (2011), which does fit the profile for the metamorphic clast lithotypes. It must be considered that the Hongliuhe Group is fault bound and that considerable strike-slip faulting has affected the entire Beishan region (Xiao et al., 2011). One of the other numerous nearby arcs (Fig. 2) may have been the source. The conglomerates up-section in Hongliuhe Group consisting of mostly unstrained granitoid boulder with volcanic cobble clasts, yields few clues to the provenance, as most arcs involved with the Mazongshan arc experienced orogenesis during the Carboniferous. Isotopic geochronological studies of the Hongliuhe Group sediments may yield more decisive clues.

4.4 Fold and Thrust Belt Style Deformation

The structures described in this study, considered at the scale of the entire Group, resemble a fold-and-thrust belt style of deformation (Price, 1981; Butler, 1982, 1987; Poblet and Lisle, 2011). The faults in the Hongliuhe area (Fig. 4) verge steeply south, showing a north-over-south sense of motion in a dominantly dip-slip fashion. Folding occurrences appear spatially linked with fault zones and the map patterns suggest their concurrent generation with faulting.

Though the faults in the Hongliuhe area are steep, their vergence matches that of the Xingxingxia structural cross-section. The Xingxingxia structural cross-section shows classic thin skinned fold-and-thrust belt style deformation (Coward, 1983), and there is no reason to believe that deformation in the Hongliuhe area is thick skinned. Figure 28 shows a schematic diagram of a foreland thrust system. Observation of the slightly higher degree of metamorphism

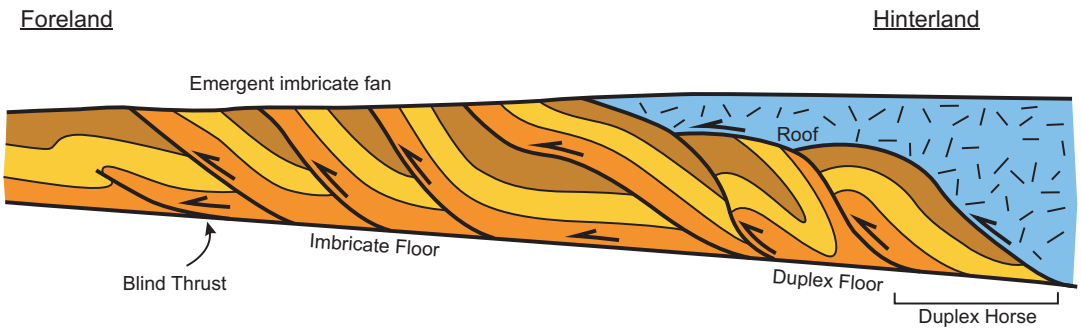

Figure 28: Schematic diagram showing the anatomy of a foreland thrust system. The geometry of faulting allows for exposed sections of steeper faulting and shallower thrust sets, both of which can be seen in the Hongliuhe Group. (Based on Figure 1 of Butler, 1987).

and involvement of crystal-plastic deformation in the shear zones of the Hongliuhe area, versus the lithologies of the Xingxingxia cross-section, lead to interpretation that the Hongliuhe area was formed in deeper sections of the thrust belt. This would be similar to any of the steeply dipping sections on the hinterland side of the thrust belt depicted in Figure 28. The lithologies of the Xingxingxia cross-section show minimal metamorphism and low-angled thrust systems, suggesting that their position in the thrust belt is more to the shallower foreland side (Fig. 28).

4.4.1 Evidence for Concurrent Faulting and Folding

The eye-fold structure in the center of the map (Fig. 5) is postulated to be a sheath fold based on its steeply plunging east and west fold axes (Fig. 20) and proximity to brittle/ductile fault zones at its north and south bounds (Skjernaa, 1989; Alsop and Holdsworth, 2006; Alsop et al., 2007). The high aspect ratio of the elliptical bedding traces in the sheath fold, and the variance from lower to high aspect ratios towards the center (Fig. 21), implies an association with a ductile shear zone in the formation of the sheath fold (Alsop et al., 2007). “Sheath folds are more likely to develop in constrictional non-coaxial shear zones” (Jiang and Williams, 1999).

Development of the sheath fold, even as a modification of a pre-existing or concurrently developing structure, would require significant displacement across the fault. The fold axes of the eastern and western halves of the sheath fold plunge very steeply towards each other. The eastern fold axis has rotated towards parallelism with the down-dip lineations of the Northern Internal Fault, implying deformation in a shear zone with a high ratio of angular shear to shortening rates (Kuiper et al., 2007). The Fry diagram produced on a deformed conglomerate from the Northern Internal Fault Zone (Fig. 18) shows not only flattening deformation, but also a strain ellipse at an angle to the stretching direction. This correlates to the north-over-south fault movement and implies simple shear is involved in the shear zone, an interpretation supported by observations of asymmetrically mantled porphyroclasts. All of these pieces of evidence provide an interpretation that the fault zones in the Hongliuhe Group accommodated significant, yet unquantified, north-over-south dip-slip displacement. This, in turn, supports the assumptions made to reconstruct the stratigraphy of the Hongliuhe Group (Fig. 6).

The magnitude of fault displacement in the Xingxingxia cross-section is unknown for most of the faults, but cross-section restoration (Fig. 27) does allow for a minimum estimate of the orogenic contraction (Hossack, 1979). The minimum estimate is a shortening to 75.8% of its original, undeformed length ($e = -0.242$).

4.5 Structural Vergence and Subduction Polarity

Structural vergence of faulting and folding in the Hongliuhe Group is consistently southward directed throughout both the mapped area and the Xingxingxia structural cross-section. Fault motion is north-over south, with consistent down-dip lineation orientations. This implies a southward directed transport direction of lithological material associated with contraction of the unit, which in turn confers a larger scale implication:

> Use of thrust vergence to define subduction polarity is often possible, if one avoids complications caused, first, by the presence of back-thrusts inherited from the oceanic domain (e.g. where there has been double subduction as in the Moluccas), or of syn- to post-accretionary back-thrusts, and second by overprinting of synsubduction, accretionary thrusts by later imposed structures. (Windley et al., 2007)

The structures examined in this study show no significant back-thrusts, and later deformation than that in the Permian is known to be confined to strike-slip motion along large-scale transcurrent faults (Xiao et al., 2011). The deformation style and tectonic setting of the Hongliuhe

Group, when considered with the strong southward structural vergence of its structures, implies a north-dipping subduction system associated with the collisional orogenic event involved in its petrogenesis.

4.6 Implications for the Beishan Orogenic Collage

The implications of a foreland fold-and-thrust belt within the terrane boundaries of the Mazongshan arc terrane are that, prior to the Hongliuhe Group's deposition in the Early Permian, a tectonic collision initiated between two of the (composite) arc terranes in the Gongpoquan arc-accretionary complex. The most probable terrane that could be involved in the collision is the Mazongshan arc terrane, as its metamorphic rocks provide the backstop of the hinterland, or overriding plate. (The following provides a quick review of more detailed tectonic context from Xiao et al. (2011), and referring to Figure 3 is very helpful to follow this sequence: the Mazongshan arc had been amalgamated with the Hanshan arc and the Shuangyingshan-Huaniushan composite arc by the Devonian period which created the Phase II Gongpoquan arc-accretionary system. The Gongpoquan composite arc then accreted the Heiyingshan arc on the north side of the previously-accreted Mazongshan terrane, by late Carboniferous. This event induced a back-arc response in the Phase III Gongpoquan arc accretionary complex, creating the Hongliuhe ocean. Final tectonic closure was brought about from north dipping subduction under the south end of the Gongpoquan in the Late Carboniferous–Early Permian.) As mentioned earlier, there has been considerable strike-slip movement of terranes in the Beishan (Xiao et al., 2011). The fault bounding the Hongliuhe Group to the north is not a major crustal-scale strike-slip fault (such as the Xingxingxia fault further north, or the Hongliuhe mélange zone), but a subsidiary fault. Under this assumption, the reasonable interpretation that the Mazongshan arc was the immediate hinterland, in whatever composite stage it was in, leads to the question: what is the foreland terrane? The tectonic models of Xiao et al. (2011) imply the Hongliuhe ocean basin opened as a back-arc response to southward directed subduction under the Gongpoquan arc-accretionary system, yet it does not indicate subduction of the Hongliuhe ocean during the late Carboniferous to Early Permian. It is possible that the Hongliuhe Group formed as a foreland basin in the back-arc setting and that compression from the outboard subduction system closed the Hongliuhe ocean and created the foreland fold-and-thrust belt in the Group. It is also possible, perhaps more so, that a subduction system was active in the Hongliuhe ocean, subducting northward under the Gongpoquan arc-accretionary system, and that collision with one of (or a composite of) the Beishan terranes – since translated to a cryptically distal position, from Triassic strike-slip motion (Xiao et al., 2011) – occurred just before deposition of the Hongliuhe Group, in the Early Permian. The involvement of some degree of strike-slip displacement along the Hongliuhe mélange zone is

supported by the consistent and strong southward structural vergence of folding and faulting in the Hongliuhe Group which is not seen in the terranes on the south side of the Hongliuhe mélange zone (Xiao et al., 2004b).

4.7 Implications for the Central Asian Orogenic Belt

A foreland fold-and-thrust belt in the Gongpoquan arc-accretionary system has many implications for the larger scale Central Asian Orogenic Belt. The Hongliuhe Group as a foreland fold-and-thrust belt inherently implies subduction and collision between terranes, but its limited spatial extent implies that the collision was smaller scale than the whole orogenic belt. This is a small but significant piece of evidence supporting the island archipelago model for the CAOB. The recognition of another foreland basin adds another constraint on the timing of final accretion of all terranes in the CAOB, though more work needs to be done to elucidate the foreland terrane. Its indistinguishable foreland terrane is evidence of large-scale strike-slip motion in the Beishan, a problem that is endemic to research in many parts of the CAOB and is glossed over in many interpretations and models.

5 Conclusion

With stratigraphic reconstruction of faulted stratigraphy the Hongliuhe Group exhibits sedimentological organization and characteristics consistent with a progressively deepening foreland depositional setting. The Group was unconformably deposited on basic volcanic rocks. The conglomeratic units towards the base are polymictic, and clast type changes to monomictic granitoid up-section, illustrating the unroofing sequence of the provenance. The presence of a large-scale sheath fold in its mid-section strata with steeply plunging fold axes implies prolonged dip-slip fault displacement over its steeply-dipping northerly bounding fault. The measure of increasing ellipticity of bedding traces towards the center of the sheath fold further suggests that the shear zones involved had high shear strain rates with respect to the shortening rate, as shown in deformed conglomerate outcrops. Deformed clasts exhibit a strain ellipse of aspect ratio 2.25 : 1 for the principal strain axes. This prolonged shearing juxtaposed older blocks of strata in the northern hangingwalls against younger blocks in the southward footwalls. Low angled southward-verging thrusts and folds in the Xingxingxia cross-section give a conservative minimum estimate of orogenic contraction to 76% of its original, undeformed length, calculated from cross-section reconstruction. The deformation reported in the Hongliuhe Group from this study is consistent with thin-skinned fold-and-thrust belt style deformation.

The presence of an Early Permian foreland fold-and-thrust belt in the Gongpoquan composite arc system, in the Beishan orogenic collage, indicates that a tectonic collision, with (at least) the Mazongshan arc terrane as the hinterland and an unknown terrane as the foreland, occurred in the Late Carboniferous to Early Permian. The vergence of the structures in the Hongliuhe Group is consistently southward, a finding which strongly implies a north-dipping subduction system involved in the final stages of this amalgamation.

References

Allen, M. B., A. M. C. Şengör, and B. A. Natal'in, 1995: Junggar, Turfan and Alakol basins as Late Permian to ?Early Triassic extensional structures in a sinistral shear zone in the Altaid orogenic collage, Central Asia. *Journal of the Geological Society, London*, **152**, 327–338.

Allen, M. B., B. F. Windley, and Z. Chi, 1992: Palaeozoic collisional tectonics and magmatism of the Chinese Tien Shan, central asia. *Tectonophysics*, **220**, 89–115.

Alsop, G. I. and R. E. Holdsworth, 2006: Sheath folds as discriminators of bulk strain type. *Journal of Structural Geology*, **28**, 1588–1606.

Alsop, G. I., R. E. Holdsworth, and K. J. W. McCaffrey, 2007: Scale invariant sheath folds in salt, sediments and shear zones. *Journal of Structural Geology*, **29**, 1585–1604.

Briggs, S. M., A. Yin, C. E. Manning, Z.-L. Chen, and X.-F. Wang, 2009: Tectonic development of the southern Chinese Altai Range as determined by structural geology, thermobarometry, $^{40}Ar/^{39}Ar$ thermochronology, and Th/Pb ion-microprobe monazite geochronology. *Geological Society of America Bulletin*, **121 (9/10)**, 1381–1393.

Buckman, S. and J. C. Aitchison, 2004: Tectonic evolution of Palaeozoic terranes in West Junggar, Xinjiang, NW China. *Geological Society, Longon, Special Publications*, **226**, 101–129.

Butler, R. W. H., 1982: The terminology of structures in thrust belts. *Journal of Structural Geology*, **4 (3)**, 239–245.

Butler, R. W. H., 1987: Thrust sequences. *Journal of the Geological Society, London*, **144**, 619–634.

Charvet, J., L.-S. Shu, and S. Laurent-Charvet, 2007: Paleozoic structural and geodynamic evolution of eastern Tianshan (NW China): welding of the Tarim and Junggar plates. *Episodes: International Union of Geological Sciences*, **30 (3)**, 162–186.

Chen, C.-M., H.-F. Lu, D. Jia, D.-S. Cai, and S.-M. Wu, 1999: Closing history of the southern Tianshan oceanic basin, western China: an oblique collisional orogeny. *Tectonophysics*, **302**, 23–40.

Coleman, R. G., 1989: Continental growth of northwest china. *Tectonics*, **8 (3)**, 621–635.

Covey, M., 1986: The evolution of foreland basins to steady state: evidence from the western Taiwan foreland basin. *Special Publications, International Association of Sedimnetologists*, **8**, 15–39.

Coward, M. P., 1983: Thrust tectonics, thin skinned or thick skinned, and the continuation of thrusts to deep in the crust. *Journal of Structural Geology*, **5 (2)**, 113–123.

Crespi, J. M., 1986: Some guidelines for the practical application of Fry's method of strain analysis. *Journal of Structural Geology*, **8 (7)**, 799–808.

Cross, T. A., 1986: Tectonic controls of foreland basin subsidence and Laramide style deformation, western United States. *Special Publications, International Association of Sedimnetologists*, **8**, 15–39.

Dahlstrom, C. D. A., 1969: Balanced cross sections. *Canadian Journal of Earth Sciences*, **6**, 743–757.

DeCelles, P. G. and K. A. Giles, 1996: Foreland basin systems. *Basin Research*, **8**, 105–123.

Dunne, W. M., C. M. Onasch, and R. T. Williams, 1990: The problem of strain-marker centers and the Fry method. *Journal of Structural Geology*, **12 (7)**, 933–938.

Erslev, E. A., 1988: Normalized center-to-center strain analysis of packed aggregates. *Journal of Structural Geology*, **10 (2)**, 201–209.

Fry, N., 1979a: Density distribution techniques and strained length methods for determination of finite strains. *Journal of Structural Geology*, **1 (3)**, 221–229.

Fry, N., 1979b: Random point distributions and strain measurement in rocks. *Tectonophysics*, **60**, 89–105.

Gao, J., M.-S. Li, X.-C. Xiao, Y.-Q. Tang, and G.-Q. He, 1998: Paleozoic tectonic evolution of the Tianshan Orogen, northwestern China. *Tectonophysics*, **287**, 213–231.

Hossack, J. R., 1979: The use of balanced cross-sections in the calculation of orogenic contraction: A review. *Journal of the Geological Society, London*, **136**, 705–711.

Jiang, D.-Z. and P. F. Williams, 1999: When do dragfolds not develop into sheath folds in shear zones? *Journal of Structural Geology*, **21**, 577–583.

Kuiper, Y. D., D.-Z. Jiang, and S.-F. Lin, 2007: Relationship between non-cylindrical fold geometry and the shear direction in monoclinic and triclinic shear zones. *Journal of Structural Geology*, **29**, 1022–1033.

Laurent-Charvet, S., J. Charvet, P. Monié, and L.-S. Shu, 2003: Late paleozoic strike-slip shear zones in eastern central Asia (NW China): New structural and geochronological data. *Tectonics*, **22 (2)**, 1009.

Laurent-Charvet, S., J. Charvet, L.-S. Shu, R.-S. Ma, and H.-F. Lu, 2002: Palaeozoic late collisional strike-slip deformations in Tianshan and Altay, Eastern Xinjiang, NW China. *Terra-Nova*, **14**, 249–256.

Li, J.-B., X. Kang, T. Wang, W.-P. Li, and Y. Tong, 2006: Establishment of the early permian hongliuhe group in the beishan area on the border region of xinjian and gansu, china. *Acta Petrologica Sinica*, **25 (4)**, 465–468 (in Chinese with English abstract).

Li, Y.-J., Z.-M. Wang, H.-R. Wu, Z.-B. Huang, Z.-J. Tan, and J.-C. Luo, 2002: Discovery of Radiolarian Fossils from the Aiketik Group at the Western End of the South Tianshan Mountains of China and Its Implications. *Acta Geologica Sinica*, **76 (2)**, 146–154.

Pan, J.-H., Z.-J. Guo, C. Liu, and Z.-H. Zhao, 2008: Geochronology, geochemistry and tectonic implications of permian basalts in hongliuhe area on the border between xinjian and gansu. *Acta Petrologica Sinica*, **24 (4)**, 793–802 (in Chinese with English abstract).

Poblet, J. and R. J. Lisle, 2011: Kinematic evolution and structural styles of fold-and-thrust belts. *Geological Society, London, Special Publications*, **349**, 1–24.

Price, R. A., 1981: The cordilleran foreland thrust and fold belt in the southern Canadian Rocky Mountains. *The Geological Society, London, Special Publications*, **9**, 427–448.

Şengör, A. M. C. and B. A. Natal'in, 2007: *Magmatism and Metallogeny of the Altai and Adjacent Large Igneous Provinces with an Introductory Essay on the Altaids: Eduard Suess and the Altaids: what is in a name?* CERCAMS/NHM.

Şengör, A. M. C., B. A. Natal'in, and V. S. Burtman, 1993: Evolution of the Altaid tectonic collage and Palaeozoic crustal growth in Eurasia. *Nature*, **364**, 299–307.

Skjernaa, L., 1989: Tubular folds and sheath folds: definitions and conceptual models for their development, with examples from the Grapesvare area, northern Sweden. *Journal of Structural Geology*, **11 (6)**, 689–703.

Thorbjornsen, K. L. and W. M. Dunne, 1997: Origin of a thrust-related fold: geometric vs kinematic tests. *Journal of Structural Geology*, **19 (3-4)**, 303–319.

Treagus, S. H. and J. E. Treagus, 2002: Studies of strain and rheology of conglomerates. *Journal of Structural Geology*, **24**, 1541–1567.

Ver Straeten, C. A., 2010: Lessons from the foreland basin: Northern Appalachian basin perspectives on the Acadian orogeny. *Geological Society of America Memoirs*, **206**, 251–282.

Wang, T., D.-W. Hong, B.-M. Jahn, Y. Tong, Y.-B. Wang, B.-F. Han, and X.-X. Wang, 2006: Timing, Petrogenesis, and Setting of Paleozoic Synorogenic Intrusions from the Altai Mountains, Northwest China: Implications for the Tectonic Evolution of an Accretionary Orogen. *The Journal of Geology*, **114**, 735–751.

Wang, Z.-H., S. Sun, J.-L. Li, Q.-L. Hou, K.-Z. Qin, W.-J. Xiao, and J. Hao, 2003: Paleozoic tectonic evolution of the northern Xinjiang, China: Geochemical and geochronological constraints from the ophiolites. *Tectonics*, **22 (2)**, 1014.

Wickham, J. and G. Moeckel, 1997: Restoration of structural cross-sections. *Journal of Structural Geology*, **19 (7)**, 975–986.

Windley, B. F., D. Alexeiev, W.-J. Xiao, A. Kröner, and G. Badarch, 2007: Tectonic models for accretion of the Central Asian Orogenic Belt. *Journal of the Geological Society, London*, **164**, 31–47.

Windley, B. F., M. B. Allen, C. Zhang, Z.-Y. Zhao, and G.-R. Wang, 1990: Palaeozoic accretion and Cenozoic redeformation of the Chinese Tien Shan range, Central Asia. *Earth Planetary Science Letters*, **45**, 326–336.

Windley, B. F., A. Kröner, J.-H. Guo, G.-S. Qu, Y.-Y. Li, and C. Zhang, 2002: Neoproterozoic to Paleozoic Geology of the Altai Orogen, NW China: New Zircon Age Data and Tectonic Evolution. *The Journal of Geology*, **110**, 719–737.

Xiao, W.-J., B. F. Windley, G. Badarch, S. Sun, J. Li, K. Qin, and Z. Wang, 2004a: Paleozoic accretionary and convergent tectonics of the southern Altaids: implications for the growth of Central Asia. *Journal of the Geological Society, London*, **161**, 339–342.

Xiao, W.-J., B. F. Windley, J. Hao, and M.-G. Zhai, 2003: Accretion leading to collision and the Permian Solonker suture, Inner Mongolia, China: Termination of the central Asian orogenic belt. *Tectonics*, **22 (6)**, 1069.

Xiao, W.-J., L. Zhang, K.-Z. Qin, S. Sun, and J.-L. Li, 2004b: Paleozoic accretionary and collisional tectonics of the eastern Tianshan (China): implications for the continental growth of Central Asia. *American Journal of Science*, **304**, 370–395.

Xiao, W.-J., et al., 2008: Middle Cambrian to Permian subduction-related accretionary orogenesis of Northern Xinjiang, NW China: Implications for the tectonic evolution of Central Asia. *Journal of Asian Earth Sciences*, **32**, 102–117.

Xiao, W.-J., et al., 2009a: End-Permian to mid-Triassic termination of the accretionary processes of the southern Altaids: implications for the geodynamic evolution, Phanerozoic continental growth, and metallogeny of Central Asia. *International Journal of Earth Sciences*, **98**, 1188–1217.

Xiao, W.-J., et al., 2009b: Paleozoic multiple subduction-accretion processes of the southern Altaids. *American Journal of Science*, **309**, 221–270.

Xiao, W.-J., et al., 2011: Paleozoic multiple accretionary and collisional processes of the Beishan orogenic collage. *American Journal of Science*, **Article in press: DOI 10.2475/04.2010.00**.

Yakubchuk, A., 2004: Architecture and mineral deposit settings of the Altaid orogenic collage: a revised model. *Journal of Asian Earth Sciences*, **23**, 761–779.

Zhang, C., M.-G. Zhai, M. B. Allen, A. D. Saunders, G.-R. Wang, and X. Huang, 1993: Implications of Palaeozoic ophiolites from Western Junggar, NW China, for the tectonics of central Asia. *Journal of The Geological Society, London*, **150**, 551–561.